

Receptor architecture of macaque and human early visual areas: not equal, but comparable

Lucija Rapan^{1*}, Meiqi Niu^{1*}, Ling Zhao¹, Thomas Funck¹, Katrin Amunts^{1,2}, Karl Zilles[†],
Nicola Palomero-Gallagher^{1,2,3}

¹ Institute of Neuroscience and Medicine (INM-1), Research Centre Jülich, Jülich, Germany

² C. & O. Vogt Institute for Brain Research, Heinrich-Heine-University, 40225 Düsseldorf, Germany

³ Department of Psychiatry, Psychotherapy, and Psychosomatics, Medical Faculty, RWTH Aachen

* These authors contributed equally

† Deceased 26th April 2020

Corresponding authors: Lucija Rapan
Institute of Neuroscience and Medicine (INM-1)
Research Centre Jülich
52425 Jülich
Germany
Phone: +49 2461 61-96746
e-mail: l.jankovic-rapan@fz-juelich.de
ORCID: 0000-0002-6582-5826

Corresponding authors: Meiqi Niu
Institute of Neuroscience and Medicine (INM-1)
Research Centre Jülich
52425 Jülich
Germany
Phone: +49 2461 61-96739
e-mail: m.niu@fz-juelich.de
ORCID: 0000-0001-7937-5814

Corresponding authors: Nicola Palomero-Gallagher
Institute of Neuroscience and Medicine (INM-1)
Research Centre Jülich
52425 Jülich
Germany
Phone: +49 2461 61-4790
e-mail: n.palomero-gallagher@fz-juelich.de
ORCID: 0000-0003-4463-8578

Keywords: brain mapping, cytoarchitecture, comparative analysis, visual processing, homology

Abstract

Existing cytoarchitectonic maps of the human and macaque posterior occipital cortex differ in the number of areas they display, thus hampering identification of homolog structures. We applied quantitative in vitro receptor autoradiography to characterize the receptor architecture of the primary visual and early extrastriate cortex in macaque and human brains, using previously published cytoarchitectonic criteria as starting point of our analysis. We identified 8 receptor architectonically distinct areas in the macaque brain (mV1d, mV1v, mV2d, mV2v, mV3d, mV3v, mV3A, mV4v), and their respective counterpart areas in the human brain (hV1d, hV1v, hV2d, hV2v, hV3d, hV3v, hV3A, hV4v). Mean densities of 14 neurotransmitter receptors were quantified in each area, and ensuing receptor fingerprints used for multivariate analyses. The 1st principal component segregated macaque and human early visual areas differ. However, the 2nd principal component showed that within each species, area-specific differences in receptor fingerprints were associated with the hierarchical processing level of each area. Subdivisions of V2 and V3 were found to cluster together in both species and were segregated from subdivisions of V1 and from V4v. Thus, comparative studies like this provide valuable architectonic insights into how differences in underlying microstructure impact evolutionary changes in functional processing of the primate brain and, at the same time, provide strong arguments for use of macaque monkey brain as a suitable animal model for translational studies.

Introduction

The visual modality is possibly the most developed in the primate brain, and occupies the largest amount of cerebral cortex ([Van Essen, 2003](#)). In primates, the early visual cortex also provides an ideal model for understanding the entire visual system in general, because of the hierarchical progression in its structural and functional organization. Within the primary visual cortex (V1), optic fibers carrying information from the lower and upper visual fields terminate on the dorsal and ventral banks of the *cas*, respectively ([Gillen, 2015](#)), and information provided by this segregation is carried on to higher visual areas, which were therefore categorized as belonging to one of two major visual streams ([Ungerleider, 1982](#)), i.e., dorsal (occipitoparietal) and ventral (occipitotemporal) streams. Overall, the simple definition of the original dorsal/ventral dichotomy resulted in a too restraining idea of a spatial and object-related perception of the dorsal and ventral flow, and it has therefore been suggested that visual information is conveyed between two systems at multiple stages and locations along the processing way. Hierarchical organization of the visual processing would be composed of multiple, intertwined processing streams, which, at a lower level, are related to the compartmental organization of early visual areas (V1-V3) and, at a higher level, are associated with the distinction between processing centers of the parietal and temporal cortex (Cloutman, 2013) (Felleman and Van Essen, 1991).

Comparative studies of the human and macaque visual system showed that the early visual areas V1, V2 and V3 are located more posterior and medially in humans than the correspondingly marked areas in macaques. This is particularly true for V1, which in humans is located almost entirely in the *cas*, whereby macaque V1 occupies a substantial portion of the operculum on the lateral surface of the occipital lobe ([Orban et al., 2004](#); [Schira et al., 2012](#)). However, early and mid-level visual areas have also been shown to be evolutionarily well-preserved, and to share a similar retinotopic organization, as well as basic functional traits across the primate species ([Denys et al., 2004](#); [Orban et al., 2003](#); [Orban et al., 2004](#); [Vanduffel et al., 2002](#)). Although the receptor architecture of areas V1-V3, including their dorsal and ventral subdivisions, as well as of adjoining areas V3A dorsally and V4 ventrally has been comprehensively characterized in the human brain ([Eickhoff et al., 2008](#); [Eickhoff et al., 2007](#)) and these early visual areas were also part of a study on the organizational principles of the human brain as revealed by regional and laminar differences in receptor densities ([Zilles and Palomero-Gallagher, 2017b](#)), the macaque monkey visual cortex has not yet been subject of such detailed receptor architectonic analyses, since existing studies concentrated mainly on macaque areas V1 and V2, analyzed only a single sample, examined a few receptor types, mostly from a single neurotransmitter system, or did not provide quantitative data

(e.g., (Hendry et al., 1990; Kötter et al., 2001; Rakic et al., 1988; Rakic and Lidow, 1995; Rosier et al., 1993; Rosier et al., 1991; Zilles and Clarke, 1997; Zilles and Palomero-Gallagher, 2017a)).

Since transmitter receptors are key molecules of signal processing in the nervous system and determine the excitatory or inhibitory effect of neurotransmitters, they are a crucial prerequisite for understanding functional neuroanatomy. Neurotransmitter receptors are heterogeneously distributed throughout the cortex, and differences in receptor densities not only reveal cortical borders, but also segregate brain regions belonging to different cortical types (i.e. allocortex vs. isocortex) and functional systems (primary motor, somatosensory, visual, or auditory; language-related vs. non-language related), and also identify hierarchical processing levels within a given functional system (Palomero-Gallagher and Zilles, 2019; Zilles et al., 2015a; Zilles and Palomero-Gallagher, 2017b). Furthermore, receptor autographic studies have also been shown to provide valuable insights into putative homologies between areas of the human and macaque monkey brain (Impieri et al., 2018; Niu et al., 2021; Palomero-Gallagher et al., 2013; Rapan et al., 2021).

Aim of the present study is to characterize transmitter expression in the primary visual cortex and in early extrastriate visual areas of the macaque brain and compare them to those of the human brain in order to identify the molecular basis of the systemic coherence of visual areas and provide a more comprehensive insight into the evolutionary aspect of the functional organization of the visual system in primates. Specifically, we addressed the following questions: a) does the multi-receptor architecture of early visual areas reveal dorso-ventral differences in the non-human primate cortex, in the same manner as it does in humans (Eickhoff et al., 2008); and b) do receptor fingerprints facilitate identification of similarities and differences between the macaque and human early visual areas?

Material and Methods

Subjects

We examined three adult male macaque monkey brains (*Macaca fascicularis*; brains ID: 11530, 11539, 11543; 6 ± 1 years of age; obtained from Covance Laboratories, Münster, Germany) for a combined cyto- and receptor architectonic analysis. Monkeys were sacrificed by a lethal intravenous injection of sodium pentobarbital and brains were immediately extracted together with meninges and blood vessels to preserve cortical layer I. The procedures used in this study had the approval of the Institutional Animal Care and Use Committee, were carried out in accordance with the European and local Committees, and complied with the European Communities Council Directive 2010/63/EU.

Further, we used a total of five post-mortem human brains from donors (76 ± 3 years of age; 3 males) without a history of neurological or psychiatric diseases and obtained through the body donor program of the Department of Anatomy, University of Düsseldorf, Germany. Causes of death were sudden cardiac failure, multiorgan failure caused by sepsis and pneumonia, and lung oedema.

Tissue processing

The macaque brains were divided into left and right hemispheres (including cerebellum with brainstem) and further separated into an anterior and a posterior slab at the height of the most caudal part of the central sulcus. Human brains were removed at autopsy and divided into left and right hemispheres. Each hemisphere was then cut into slabs of approximately 3cm each. All slabs were shock frozen in N-methylbutane (isopentane) at -40°C for 10 – 15 minutes, and serially sectioned (thickness 20 μm) in the coronal plane with a cryotome at -20°C , thaw-mounted on gelatin-coated glass slides, air dried and stored overnight at -20°C .

In order to examine the laminar and regional distribution patterns of 14 receptor types belonging to the classical neurotransmitters glutamate (AMPA, kainate and NMDA), GABA (GABA_A , GABA_A/BZ and GABA_B), acetylcholine (muscarinic M_1 , M_2 and M_3), noradrenaline (α_1 and α_2), serotonin (5-HT_{1A} and 5-HT₂) and dopamine (D_1), and to enable comparison with cytoarchitectonic features, alternating sections were processed for quantitative in vitro receptor autoradiography according to previously published protocols (Palomero-Gallagher and Zilles, 2018; Zilles et al., 2002), or for visualization of cell-bodies with a modified silver cell-body staining (Merker, 1983) that provides a high contrast between cell bodies and neuropil. The

radiolabelled sections were then air-dried and exposed against tritium-sensitive films (Hyperfilm, Amersham, Braunschweig, Germany) together with plastic tritium standards of known radioactivity concentrations (Microscales®, Amersham) for 4-18 weeks. The ensuing autoradiographs reveal the regional and laminar distribution of receptor binding sites.

Image acquisition and analysis

Histological sections were scanned by means of a light microscope (Axioplan 2 imaging, ZEISS, Germany) equipped with a motor-operated stage controlled by the KS400® and Axiovision (Zeiss, Germany) image analyzing systems applying a 6.3 x 1.25 objective (Planapo®, Zeiss, Germany), and a CCD camera (Axiocam MRm, ZEISS, Germany) producing frames of 524 x 524 µm in size, 512 x 512-pixel spatial resolution, with an in-plane resolution of 1 µm per pixel, and eight-bit grey resolution. These digitalized serial images were used for the qualitative cytoarchitectonic identification of distinct occipital areas in the macaque monkey brains.

Autoradiographs were digitized with an image analysis system consisting of a source of homogenous light and a CCD-camera (Axiocam MRm, Zeiss, Germany) with an S-Orthoplanar 60-mm macro lens (Zeiss, Germany) corrected for geometric distortions, connected to the image acquisition and processing system Axiovision (Zeiss, Germany), in order to carry out densitometric analysis of binding site concentrations in the radioactive sections ([Palomero-Gallagher and Zilles, 2018](#); [Zilles et al., 2002](#)). Spatial resolution of the resulting images was 3000 x 4000 pixels (8-bit grey value resolution). Because these images only code grey values, which represent concentration levels of radioactivity, a scaling (i.e. a linearization of the digitized autoradiographs) was carried out to transform the grey values into fmol binding sites/mg protein using in house developed Matlab (The MathWorks, Inc. Natick, MA) scripts. To provide a clear visualization of the regional and laminar receptor distribution patterns, digitized autoradiographs were linearly contrast enhanced and pseudo-colour coded.

Receptor densities of each area were extracted from the linearized images by computing the surface below profiles defined vertically to the cortical surface using in house developed scripts for Matlab (The MathWorks, Inc. Natick, MA) as previously described ([Palomero-Gallagher et al., 2008](#); [Palomero-Gallagher and Zilles, 2018](#)). Location of measuring sites, and assignment to a cytoarchitectonically identified area was ensured by comparison of the autoradiographs with the adjacent cell-body stained sections.

Identification of cortical areas

Selection of regions of interest for extraction of receptor densities in both macaque and human early visual areas was based on the architectonic identification of areas according to previously published criteria, and the analysis of multiple receptors in adjacent sections from the same brains. Specifically, in the macaque brain, areas V1-V3 and their subdivisions, as well as area V3A, dorsally and V4v ventrally were identified according to previously published cytoarchitectonic criteria and cortical maps (Felleman and Van Essen, 1991; Niu et al., 2020; Van Essen et al., 1986). Areas marked as V3 and VP (Felleman and Van Essen, 1991) correspond to our V3 subdivisions, mV3d and mV3v respectively. A large portion of macaque V1 is also found on the lateral surface of the hemisphere, whereas human V1 is mainly located within the calcarine sulcus (Schira et al., 2012). Since retinotopic mapping has shown that the lower and upper visual fields are represented on the lateral surface in same manner as within the calcarine sulcus (Rosa, 2002), we here concentrated on the sulcal portion of macaque V1

In the human brain, areas V1 and V2 were identified according to Amunts et al. (2000), areas hOc3v and hOc4v on the ventral occipital cortex according to Rottschy et al. (2007), and areas hOc3d and hOc4d on the dorsal occipital cortex according to Kujovic et al. (2013). Areas hOc3d and hOc4d are the putative anatomical substrates of functionally defined areas V3d and V3A, respectively (Kujovic et al., 2013), and areas hOC3v and hOC4v are those of functionally defined areas V3v and V4v, respectively (Rottschy et al., 2007). Eickhoff et al. (2008) analyzed the receptor architecture of early visual areas in the human brain and besides confirming the cytoarchitectonically defined areas, identified dorso-ventral subdivisions within areas V1 and V2. Since visual inspection of the color coded receptor autoradiographs hinted at a comparable situation in the macaque brain, for each of these areas, densities were quantified in both species in a dorsally located region of interest (i.e. V1d, V2d) and in a ventrally located region of interest (i.e. V1v, V2v).

Note, that to avoid confusion, in the present analysis the prefix m- will be used to identify all monkey areas. Furthermore, to facilitate comparison between species, for human areas we will apply the functionally relevant nomenclature, albeit with the prefix h- (e.g., hV3A for area hOc4d).

Statistical analysis of receptor densities

To determine if there were significant differences in receptor architecture between paired areas (dorsal and ventral subdivisions of the same visual region, or of adjacent areas from different

hierarchical levels), stepwise linear mixed-effects models were performed separately for human and macaque visual areas. To ensure an equal weighting of each receptor in subsequent statistical analyses, receptor density values were normalized within each receptor type separately in human and macaque by applying the min-max scaling (Eq.1).

$$z_i = \frac{x_i - \min(x)}{\max(x) - \min(x)} \quad (1)$$

where x is absolute receptor density, i represents an individual section, and z is the normalized data. Unless otherwise specified, normalization was performed separately in macaque and human data.

Statistical analyses were conducted using the R programming language ([version: 3.6.3](#); Team, 2013). For each species, the statistical testing involved three levels. In the first step, an omnibus test was carried out to determine whether there were differences across all areas when all receptor types are considered simultaneously (Eq.2). The model consisted of fixed effects for area and receptor type, and human/macaque hemisphere was set as a random factor.

$$D_{a,r,b} = \alpha_0 + \alpha_1 A_a + \alpha_2 R_r + \alpha_3 A_a R_r + \beta_1 B_b \quad (2)$$

where D is the receptor density, A is visual area, R is receptor type and B is human/macaque brain.

If the interaction effect between area and receptor type at the first step test was found to be significant, a second set of simple effect tests was performed for each receptor separately (i.e. 14 simple effect tests were performed in total) to determine whether there were significant differences across all areas for each receptor type. To correct for multiple comparisons in the second step tests, the false-discovery rate correction ([Benjamini and Hochberg, 1995](#)) was performed (i.e. p -values were corrected for 14 comparisons).

Finally, for the receptor types that were found to show significant differences across all areas in the second step tests, a third set of post hoc tests were used to explore the paired areas that drove the statistical difference. For each receptor type, 28 post hoc tests were performed. To correct for multiple comparisons in the third step tests, we performed the false-discovery rate correction ([Benjamini and Hochberg, 1995](#)) separately for each receptor type (i.e. p -values were corrected for 28 comparisons per receptor type).

Multivariate cluster analyses

For each architectonically defined early visual area, we calculated mean areal densities (i.e. averaged over all cortical layers) of each of the 14 different receptors. In order to display the densities of multiple receptors within and between different cortical areas more intuitively, the ensuing densities were visualized for each area as a “receptor fingerprint”, i.e., as a polar coordinate plot simultaneously depicting the concentrations of all examined receptor types within that area ([Palomero-Gallagher and Zilles, 2018](#); [Zilles et al., 2002](#)).

Principal components (PCA) and hierarchical cluster analyses were carried out using in house developed Matlab (The MathWorks, Inc. Natick, MA) scripts. Analyses were first carried out for macaque and human areas separately to identify the grouping of early visual areas in each species based on similarities in their receptor-architecture. Receptor densities were normalized by z-scores for each receptor and species separately to ensure an equal weighting of receptors expressed at overall high and low densities. The Euclidean distance was used in the hierarchical cluster analysis as a measure of (dis)similarity of areas since it best captures the differences in size and shape between fingerprints, and the Ward linkage algorithm was chosen as the linkage method, since in combination with the Euclidean distance it resulted in the maximum cophenetic correlation coefficient as compared to any combination of alternative linkage methods and measurements of (dis)similarity ([Palomero-Gallagher et al., 2009](#)). The optimal number of clusters, k , for the K-means algorithm was determined by clustering the data with k from 1 to 9. For each clustering of the data, the squared Euclidean distance between the data points and their respective centroids, i.e., distortion, was calculated and plotted against each k ([Rousseeuw, 1987](#)). We also sought to determine similarities between receptor types by how their expression levels varied across areas. To this purpose we transposed the matrices used for the clustering of areas based on differences in their receptor fingerprints, so that receptor densities were normalized by z-scoring for each area and species separately, and carried out a second set of PCA, hierarchical cluster and K-means analyses separately for the macaque and human brains.

Finally, to address the question of homologies between human and macaque visual areas, a species-combined PCA was conducted as previously described ([Sherwood et al., 2004](#)). Note, that prior to this PCA, a species-combined normalization was performed. That is, within each receptor, the density for all macaque and all human areas were jointly normalized by z-scores.

Results

Eight subdivisions of the early visual cortex were identified and receptor architectonically characterized in the macaque monkey (mV1d, mV2d, mV3d, mV3A, mV1v, mV2v, mV3v, and V4v; [Fig. 1](#)) and the human (hV1d, hV2d, hV3d, hV3A, hV1v, hV2v, hV3v, and hV4v) brain.

Stepwise linear mixed-effects models were performed for macaque and human brains to determine whether there were significant differences in receptor densities between adjacent pairs of areas along the visual hierarchy separately for the dorsal and ventral streams (e.g. from V1d through V2d to V3A), as well as between the dorsal and ventral components of a specific hierarchical level (e.g., V1d vs V1v), and if so, which receptor types contributed to these distinctions. The interaction effect between area and receptor type was found to be significant in the first level test ([Supplementary Table 2](#)), and second level tests for each receptor type separately revealed that density differences in all receptors except for M₁ and D₁ in macaques and GABA_B and D₁ in humans contribute to the segregation of early visual areas ([Supplementary Table 3](#)). The results of the third level tests, which served to identify which paired areas drove the statistical difference and will be described in the following paragraphs, and are listed in [Supplementary Tables 4 and 5](#) (macaque and human brains, respectively) and graphically displayed in [Fig. 2](#) and [Supplementary Figs. 4-5](#).

Cytoarchitecture and receptor distribution patterns

Subdivisions of area V1

Dorso-ventral heterogeneities were recognized in area V1 within the calcarine sulcus (*cas*) based on cytoarchitectonic differences in sublayers IVa and IVb ([Fig. 3](#); [Supplementary Fig. 1](#)). The dorsal subdivision (mV1d), has a more prominent layer IVa when compared to its ventral counterpart (mV1v). Furthermore, mV1d has more densely packed, and larger pyramids in layer IVb than does mV1v. Differences between mV1d and mV1v were confirmed by the receptor architectonic analysis ([Fig. 3](#); [Supplementary Fig. 1](#)). Lower GABA_A, GABA_B, GABA_A/BZ and M₃ receptor densities were found in the infragranular layers of mV1v than in those of mV1d, whereas the opposite holds true for the kainate, 5-HT_{1A}, and 5-HT₂ receptors. However, these differences did not reach the level of significance at the mean areal (i.e., densities averaged over all cortical layers) level.

In addition to differences between the dorsal and ventral banks of macaque V1, a modular distribution throughout macaque V1 was particularly obvious for the M₂ receptor, and to a lesser

extent for the GABA_A and 5-HT₂ receptors (Fig. 3; Supplementary Fig. 1). Furthermore, GABA_A/BZ, GABA_B, M₁, and M₂ densities are higher in the lateral than in the medial portion of mV1d, and the opposite holds true for M₃ receptors in mV1v.

V1/V2 border and subdivisions of area V2

Area mV2 is located anterior to mV1 as a continuous cortical belt (Fig. 1). The boundary between both areas is the clearest cytoarchitectonic border due to the sharp change from a tripartite layer IV in V1 to a homogeneous granular layer in V2 (Figs. 3-5; Supplementary Figs. 1-3). The border between layers II and III, as well as that between layers IV and V, is sharper in the portion of mV2 located dorsal to V1 (i.e., in mV2d) than in mV2v (Figs. 3 and 4). Significant differences in receptor architecture between V1 and V2 were found for most receptor types (Supplementary Fig. 4). Area mV2d contains lower NMDA, M₂, M₃, α_2 and 5-HT₂, but higher kainate and 5-HT_{1A} receptor densities than does mV1d. Ventrally, mV2v contains lower NMDA, GABA_A, M₂, and α_2 but higher 5-HT_{1A} receptor densities than does mV1v.

Although differences between mV2d and mV2v were evident at the laminar level, with infragranular layers of the former area presenting higher kainate, NMDA, GABA_B, and M₁ receptor concentrations than those of the latter area (Figs. 4 and 5, Supplementary Figs. 2 and 3), no significant differences were found at the mean areal level (Supplementary Fig. 4).

In the human brain we found a comparable pattern of significantly different receptor densities between adjacent subdivisions of areas V1 and V2 to that described for the macaque (Supplementary Fig. 4). NMDA, M₂, M₃, α_2 densities were also higher, and 5-HT_{1A} densities lower in hV1 than in hV2. However, kainate densities did not differ significantly between both areas in the human brain, but GABA_A densities were significantly higher in hV1 than in hV2. Furthermore, when comparing the dorsal and ventral components of V2, we found a significantly higher 5-HT₂ receptor density in hV2d than in hV2v.

V2/V3 border and subdivisions of area V3

Dorsal to mV2d, mV3d was identified within the posterior region of the sulcal complex of the *pos*, and was followed laterally by mV3A, which lies in the fundus of the *ips/pos* junction (Fig. 1). Due to inter-individual variability in the extent of area mV3d, the mV3d/mV3A border can be found either on the rostral wall of the anectant gyrus, on the apex of the gyrus, or on its posterior wall. On the ventral occipital surface, mV3v replaces mV2v between *ios* and *ots*, and is also found within these sulci. Area mV4v is located ventral and anterior to mV3v, on the rostral wall of the *ios*, and extending onto the ventrolateral surface of the hemisphere. Whereas mV3d and mV3v

from a continuous cortical belt around mV2, areas V3A and V4v do not share a common border (Fig. 1).

Areas mV3d and mV3v can be clearly delineated from mV2d and mV2v, respectively, due to the more prominent lamination, particularly concerning cell density in layer IV and the columnar differentiation in layer III, in the latter than in the former areas (Figs. 4 and 5). The clear bilaminar distribution of M₂ receptors in mV2v is no longer visible in mV3v (Fig. 4), and mean kainate receptor densities were significantly higher in mV3v than in mV2v (Figs. 4 and 5, Supplementary Fig. 4). Dorsally, mV2d contains a significantly higher kainate receptor density than does mV3d (Figs. 4 and 5, Supplementary Fig. 4).

Compared to mV3v, mV3d has a more prominent layer II and, in general, a clearer lamination (Figs. 4 and 5). These two areas also differ significantly in their kainate and 5HT_{1A} receptor densities, which are higher in mV3v than in mV3d (Figs. 4 and 5, Supplementary Figs. 2-4).

The main cytoarchitectonic difference between mV3A and mV3d is the clear sublamination of layer V in mV3A, but not in mV3d. Furthermore, a slight increase in the size of layer IIIc pyramids is noticed when moving from mV3d to mV3A (Fig. 5). For most receptor types differences between mV3d and mV3A were most prominent in the supragranular layers (Fig. 5, Supplementary Fig. 3). mV3d contains a lower 5-HT_{1A} receptor density than does mV3A (Supplementary Fig. 4).

Cytoarchitectonic analysis revealed that area mV4v has wider and more densely packed layers II and IV compared to area mV3v (Fig. 4). Furthermore, as shown in Fig. 3 and Supplementary Fig. 2, area V4v has lower AMPA and GABA_A, but higher GABA_A/BZ, GABA_B, and M₁ densities than V3v. However, only the difference in the density of AMPA receptors reached the level of significance (Supplementary Fig. 4).

In the human brain significant differences were also found between all pairs of adjacent areas belonging to the dorsal stream (Supplementary Fig. 4). As in the macaque brain, densities in hV3d were significantly lower than those in hV2d or hV3A. Within the ventral stream, and in contrast with findings in the macaque brain, no significant differences were found between hV2v and hV3v. However, as described for the macaque brain, the significantly higher densities were found in hV3v as compared to hV4v.

Multivariate analyses of receptor fingerprints

Fig. 6 shows the receptor fingerprints of areas analyzed in the present study in the early visual cortex of both macaque monkey and human brains, and [Supplementary Table 6](#) provides numeric values. The corresponding normalized data are presented in [Supplementary Fig. 6](#) and [Supplementary Table 7](#). The absolute mean receptor concentration varies considerably between the different receptor types in each area. In both species, GABA_A and GABA_B receptors, as well as GABA_A/BZ binding sites are present at the highest absolute densities, whereas lowest absolute densities are reached by the 5-HT_{1A} and D₁ receptors.

Two sets of hierarchical clustering and principal component analyses were performed with each the macaque and the human data. The first set of analyses aimed to visualize the degree of (dis)similarity in the normalized fingerprints of early visual areas ([Fig. 7](#)). The *k*-means analysis and elbow plots clearly indicated that *k*=3 provided the optimal trade-off between number of clusters and distortion for both the macaque and the human brain ([Supplementary Fig. 7](#)). The second set of analyses aimed to identify (dis)similarities between receptors in their expression levels across visual areas ([Supplementary Fig. 8](#)), and *k*=2 was found to be the optimal number of clusters for the macaque brain, whereas that for the human brain was *k*=4 ([Supplementary Fig. 9](#)).

In the macaque monkey ([Fig. 7A](#)) cluster 1 contained the two subdivisions of mV1, which separated very early from the remaining areas (cluster 2). Within cluster 2, areas mV2d, mV2v, mV3d, mV3v and mV3A are found in one group (cluster 2.1), whereas area mV4v is separated from the other early visual areas to form an isolated cluster 2.2. The segregation of clusters 1 and 2 was also confirmed by the 1st principal component of the PCA, and that of clusters 2.1 and 2.2 by the 2nd principal component ([Fig. 7A](#)). The analyses aiming to reveal which receptors can be grouped based on how their densities change across the examined areas ([Supplementary Fig. 8A](#)) indicated a segregation of AMPA, kainate, M₁, α_1 and 5-HT_{1A} receptors (cluster 2) from the remaining examined receptor types (cluster 1), which was confirmed by differences along the 1st principal component of the PCA ([Supplementary Fig. 8A](#)).

In the human brain, areas hV1d and hV1v also grouped together as a single cluster (cluster 1, [Fig. 7B](#)). Areas hV2d, hV2v, hV3d and hV3v are all found in a single cluster (cluster 2.1), and areas hV3A and hV4v are grouped in cluster 2.2. The 1st principal component of the PCA clearly segregated these three clusters, whereas the 2nd principal component more strongly reflected differences between hV2d, hV2v, hV3d and hV3v and the remaining areas ([Fig. 7B](#)). Clustering of the receptors according to variations in their distribution patterns across visual areas ([Supplementary Fig. 8B](#)) revealed four clusters: Cluster 1.1 contained the NMDA, GABA_A, M₁,

M₂, α_2 and 5-HT₂ receptors; cluster 1.2 the M₃, α_1 and D₁ receptors; cluster 2.1 the AMPA and 5-HT_{1A} receptors; cluster 2.2 the kainate and GABA_B receptors as well as the GABA_A/BZ binding sites. In the PCA, AMPA and 5-HT_{1A} were separated from the remaining receptors by differences along the 2nd principal component, whereas clusters 1.1, 1.2 and 2.2 were segregated by the 1st principal component.

Finally, to address the issue of comparability between homolog areas in each species, a species-combined PCA was performed (Fig. 8). The 1st principal component clearly segregates human and macaque areas, whereas the 2nd principal component generally reflects differences in the fingerprints associated with the hierarchical processing level of each area.

Discussion

We here present the first quantitative analysis of the distribution and inter-individual variability in the densities of 14 neurotransmitter receptors in the cytoarchitectonically identified macaque primary visual area V1, early visual areas V2d, V2v and V3v, as well as of higher visual area V4v, and compare our results with data obtained from the human brain (Eickhoff et al., 2008; Eickhoff et al., 2007; Zilles and Palomero-Gallagher, 2017b). Multivariate analyses of the receptor densities extracted from the identified areas revealed that although the receptor fingerprints of monkey early occipital areas differ from those of their counterparts in the human brain, within each species the area-specific differences in receptor densities reflected the hierarchical processing level of each area in a comparable manner.

We analyzed receptors for classical neurotransmitters because, unlike neuropeptides, classical neurotransmitters are actively involved in conveying information across a synapse, and unlike non-classical neurotransmitters, they mediate unidirectional anterograde signal transmission. With the receptors analyzed here, we cover a representative sample of the ionotropic/metabotropic and excitatory/inhibitory receptor types to which the major classical neurotransmitters glutamate, GABA, acetylcholine, noradrenaline and serotonin can bind, and which serve to explain the diversity of signal amplification and processing levels as well as time scales at which neurochemical signaling takes place in the mammalian brain (Palomero-Gallagher and Zilles, 2018). Furthermore, these receptors have been shown to be evolutionarily conserved in the primary sensory areas of human and macaque monkey brains (Zilles and Palomero-Gallagher, 2017a).

Receptor architectonic subdivisions of cytoarchitectonically identified visual areas in the macaque brain

Area V1 is the cytoarchitectonically most differentiated isocortical area in the primate brain, with a unique sublamination of layer IV (Zilles et al., 2015b). This cytoarchitectonic uniqueness is mirrored by its receptor architecture, which clearly reveals the border to V2, as revealed not only in the macaque (present results; Hendry et al., 1990; Rakic et al., 1988; Rakic and Lidow, 1995; Rosier et al., 1991; Zilles and Clarke, 1997; Zilles and Palomero-Gallagher, 2017a) but also in the vervet brain (Takemura et al., 2020).

Layer-specific differences in receptor densities enabled the definition of qualitative dorsal and ventral components of mV1 within the calcarine sulcus, as well as medio-lateral density gradients within each of these compartments. This heterogeneous receptor distribution probably represents the molecular underpinning of the fact that visual information from the upper and lower, as well as from the peripheral and central, visual fields is known to be processed separately in primate V1 (Dougherty et al., 2003; Gattass et al., 2005; Previc, 1990; Silson et al., 2018; Van Essen et al., 1986). Furthermore, since mV1d sends topographically organized projections to mV2d and mV3d, whereas mV1v projects to mV2v, but not to mV3v (Van Essen et al. 1986), this retinotopic organization is propagated through early extrastriate visual areas, and also reaches areas of the posterior inferotemporal and dorsal occipitotemporal cortex (Kolster et al., 2014; Zhu and Vanduffel, 2019).

The modular distribution of M_2 , $GABA_A$, and $5-HT_2$ receptors within macaque V1 resembles the previously described blobs and interblobs revealed by cytochrome-oxidase staining (Horton and Hubel, 1981; Wong-Riley, 1979), as well as the periodical distribution of $GABA_A$ receptors in the human brain (Zilles and Schleicher, 1993). Although the functional meaning of blobs and interblobs has been controversially discussed in the literature, they are commonly thought to be associated with differential color domains and orientation-selective processes (Lu and Roe, 2008).

Similar to V1, area V2 in the monkey has been described as a cytoarchitectonically homogeneous region (de Sousa et al., 2010), and we detected no significant differences in receptor densities at the mean areal level. However, we found a trend towards higher kainate, NMDA, $GABA_B$, and M_1 densities in the infragranular layers of mV2d, as well as higher $5HT_{1A}$ but lower M_2 concentrations in its supragranular layers than in the corresponding layers of mV2v. These qualitative differences would be in accordance with the dorso-ventral asymmetry in connectivity patterns of V2. Whereas V2d and V2v project back to V1 and forward to dorsal and ventral parts of V3 (Gattass et al., 1997), output to area V4t was found to originate in the dorsal part of V2, but not in V2v (Gattass et al., 2005; Gattass et al., 1997). Furthermore, V2 encompasses dorsal and ventral functional subdivisions in which the inferior and superior contralateral quadrants are represented, respectively (Gattass et al., 1981), and these subdivisions also differ in the length and orientation of their cytochrome oxidase positive stripes (Olavarria and Van Essen, 1997).

Cortex located immediately rostral to V2 has been designated as the “third visual complex”, and encompasses our areas V3v, V3d, and V3A (Rosa et al., 2005; Zeki, 1978), where area V3v has also been designated as area VP (de Sousa et al., 2010; Hof and Morrison, 1995; Zilles and Clarke, 1997). The receptor architecture of areas V3d and V3A, which are located at the junction of the

intraparietal and parieto-occipital sulci, was comprehensively characterized in a recent mapping study of the macaque intraparietal sulcus, and the same sample was used as for the present analysis (Niu et al., 2020). Our data confirms and expands on a study by Kötter et al. (2001) on the relationship between area-specific differences in receptor densities and connectivity patterns in multiple areas of the macaque monkey brain, including visual areas analyzed here, since their analysis of the visual cortex only included the AMPA, kainate, GABA_A, M₁, M₂ and 5-HT₂ receptors, and they only extracted densities from a single macaque hemisphere (which was not included in the present analysis).

Similarities and differences in the receptor architecture of macaque and human early visual areas

We found the fingerprints of macaque visual areas to differ in shape from those of their human homologs, indicating species-specific differences in the balance between the analyzed receptor types of the GABAergic system. E.g., whereas GABA_A/BZ binding site densities were higher than GABA_A receptor densities in mV1d and mV1v, the opposite holds true for hV1d and hV1v. Human and macaque V1 are also known to differ in their laminar distribution pattern of cytochrome oxidase activity in layers IVa and IVb, and in the organization of input from the magno- and parvocellular projections from LGN (Preuss et al., 1999) which has been interpreted as suggesting an evolutionary shift in the organization of LGN input to the primary visual cortex and reflecting different mechanisms of motion processing in humans than in non-human primates (Orban et al. 2004).

In both species, primary visual area V1 significantly differed from V2 by a higher mean density of M₂ and α_2 receptors, but a lower one 5-HT_{1A} receptors. These differences are in accordance with previous receptor architectonic reports in the human visual cortex (Eickhoff et al., 2008; Eickhoff et al., 2007; Zilles and Palomero-Gallagher, 2017b), and are also supported by qualitative descriptions in the macaque brain (Rakic et al., 1988; Rakic and Lidow, 1995). Notably, the hierarchical cluster analysis carried out to identify groupings of receptors based on (dis)similarities in their expression levels throughout visual areas revealed for both macaque and human brains that the 5-HT_{1A} receptors were located cluster 2 whereas the M₂ and α_2 receptors were in cluster 1. Additionally, in macaques V1 presented significantly higher 5-HT₂ levels than V2, whereas human V1 and V2 differed in GABA_A receptor densities, thus highlighting possible interspecies

differences in the molecular mechanisms subserving information transfer between V1 and early visual areas.

Given the differences between V1 and V2, it is not surprising that the hierarchical cluster analysis and the 1st principal component of the PCA clearly segregated the fingerprints of human and macaque primary subdivisions from the rest of the visual areas (Fig. 7). Furthermore, as shown by the combined PCA, both species have in common that segregation along the 2nd principal component reflected differences in fingerprints which are associated with the hierarchical processing level of each area. Thus, the transition that the molecular structure of early visual areas undergoes when moving from the primary visual cortex through V2 and V3, and up to V3A and V4v, is comparable in the macaque and human brains.

There were species differences, however, concerning the segregation pattern of V3A, and they were also confirmed by the hierarchical clustering analysis: in the macaque brain, mV3A clustered with mV3d, but in the human brain it was clearly separated, together with hV4v, from lower level visual areas (Fig. 7). Receptor fingerprints of hV3A and hV4v differ in shape from the rest of areas in the balance between GABA_A/BZ and GABA_B receptors, indicating functionally specific areas, which represent different hierarchical levels within the visual system. Interestingly, differences in kainate receptors were found to be significant in the monkey brain, but not human; i.e., mV3A and mV3d expressed significantly lower kainate densities than the surrounding areas. Pre- and postsynaptic kainate receptors are important for neurotransmission regulation, and seem to be involved in short- and long-term plastic phenomenon, highlighting their crucial role in synaptic signaling (Lerma, 2003).

Area V3A represents an intermediate region in visual processing between lower level areas V1-V3 and higher visual areas of the dorsal and ventral streams (Tootell et al., 1997)(Tootell et al. 1997), since it shares connections with areas in the parietal and the temporal cortex (Felleman and Van Essen 1991). Interestingly, functional studies in humans associated area V3A with motion processing (Tootell et al., 1997), while similar studies in monkeys described area V3d as being more sensitive to motion than area V3A (Tolias et al., 2001; Tootell et al., 1997; Vanduffel et al., 2001), suggesting that area V3A plays different roles in humans and monkeys (Orban et al., 2003; Orban et al., 2004; Tootell et al., 1997), and the differing clustering patterns of area V3A in the human and macaque visual systems described in the present study provide further support for this hypothesis. However, monkey V3A has a similar retinotopic organization to that of human V3A, with a complete representation of the visual field separated by the horizontal meridian (Brewer et

al., 2002; Fize et al., 2003; Gattass et al., 1988; Tootell et al., 1997), and in both species is associated with the processing of stereoscopic stimuli (Backus et al., 2001; Tsao et al., 2003). The fact that our clustering analyses did not result in a clear segregation of areas V2d, V2v, V3d and V3v could indicate that crosstalk between areas of the dorsal and ventral streams not only occurs at hierarchically higher processing levels (Van Polanen and Davare, 2015), but that there is already a strong interconnectivity between both streams at very early stages of the processing of visual stimuli.

In the macaque, area mV4v formed its own cluster, not only due to differences in the shape of fingerprints, but also to the fact that its fingerprint is the smallest of all analyzed areas. However, in humans hV4v was found to cluster with hV3A, indicating that the receptor fingerprint of mV4v differs more from those of the remaining macaque extrastriate visual areas than does hV4v from the remaining human extrastriate visual areas. This latter fact seems to be driven by species-specific differences since the overall receptor balance in hV4v is driven by the high densities of the GABAergic receptors. Primate area V4v constitutes a mid-level visual processing region that receives input primarily from area V2 and sends output to the inferior temporal cortex (Tootell et al., 1997) as well as topographically organized feedback projections to V2 and V3 (Ungerleider et al., 2008). It has been characterized as a color-sensitive area representing the dorsal half of the visual field (Felleman and Van Essen 1991; Gattass et al. 1988; Zeki 1978). A functionally comparable region was defined in the human brain based on *in vivo* retinotopic imaging (DeYoe et al., 1996; Sereno et al., 1995; Tootell et al., 1996), although a later imaging study showed that only a quarter-field is represented in hV4v (Wilms et al., 2010). However, given that the Euclidean distance between the normalized receptor fingerprints of mV4v and hV4v was the smallest of all inter-species comparisons, it is plausible to consider them homolog areas.

Concluding, we identified and characterized eight receptor architectonically distinct areas in the early visual cortex of the macaque monkey, i.e., V1d, V1v, V2d, V2v, V3d, V3v, V3A and V4v, and compared their fingerprints with those of their homologs in the human brain. Multivariate analyses revealed that although macaque and human early visual areas differ in their molecular architecture, within each species the area-specific differences in receptor fingerprints reflected comparable hierarchical processing levels. Furthermore, in both species the subdivisions of areas V2 and V3 were found to be more closely grouped, i.e., to bear a closer neurochemical resemblance to each other than to remaining areas, and were clearly segregated from the

subdivisions of the primary visual cortex and also from V4v. Thus, the macaque monkey early visual cortex can be considered as a good animal model for translational studies.

Code availability

Original code has been deposited at GitHub: https://github.com/MeiqiNiu/early-visual_human_monkey.

Data availability

The authors confirm that the data supporting the findings of this study are available within the article and its supplementary materials. The parcellation scheme and the receptor fingerprints of all examined areas are also made available to the neuroscientific community under <https://balsa.wustl.edu/study/177k6> and the Ebrains platform from the Human Brain Project (<https://search.kg.ebrains.eu/instances/Project/e39a0407-a98a-480e-9c63-4a2225ddfbe4>).

Acknowledgements

This project has received funding from the European Union's Horizon 2020 Research and Innovation Programme under the Specific Grant Agreements 785907 (Human Brain Project SGA2) and 945539 (Human Brain Project SGA3), from the Federal Ministry of Education and Research (BMBF) under project number 01GQ1902, and from the Helmholtz Association's Initiative and Networking Fund through the Helmholtz International BigBrain Analytics and Learning Laboratory (HIBALL) under the Helmholtz International Lab grant agreement InterLabs-0015.

Conflicts of interest

The authors have no conflicts to declare

Author contributions

Lucija Rapan – Conceptualization, Investigation, Data Curation, Visualization, Writing – Original Draft, Writing – Review and Editing

Meiqi Niu – Conceptualization, Investigation, Data Curation, Visualization, Writing – Original Draft, Writing – Review and Editing

Ling Zhao – Formal Analysis, Writing – Review and Editing

Thomas Funck – Formal analysis, Writing – Review and Editing

Katrin Amunts – Writing – Review and Editing

Karl Zilles – Conceptualization, Resources, Supervision

Nicola Palomero-Gallagher – Conceptualization, Writing – Review and Editing

References

- Amunts, K., Malikovic, A., Mohlberg, H., Schormann, T., and Zilles, K. (2000). Brodmann's areas 17 and 18 brought into stereotaxic space—where and how variable? *Neuroimage* 11, 66-84.
- Backus, B.T., Fleet, D.J., Parker, A.J., and Heeger, D.J. (2001). Human cortical activity correlates with stereoscopic depth perception. *Journal of neurophysiology* 86, 2054-2068.
- Benjamini, Y., and Hochberg, Y. (1995). Controlling the false discovery rate: a practical and powerful approach to multiple testing. *Journal of the Royal statistical society: series B* 57, 289-300.
- Brewer, A.A., Press, W.A., Logothetis, N.K., and Wandell, B.A. (2002). Visual areas in macaque cortex measured using functional magnetic resonance imaging. *Journal of Neuroscience* 22, 10416-10426.
- Cloutman, L.L. (2013). Interaction between dorsal and ventral processing streams: where, when and how? *Brain and language* 127, 251-263.
- de Sousa, A.A., Sherwood, C.C., Schleicher, A., Amunts, K., MacLeod, C.E., Hof, P.R., and Zilles, K. (2010). Comparative cytoarchitectural analyses of striate and extrastriate areas in hominoids. *Cerebral Cortex* 20, 966-981.
- Denys, K., Vanduffel, W., Fize, D., Nelissen, K., Peuskens, H., Van Essen, D., and Orban, G.A. (2004). The processing of visual shape in the cerebral cortex of human and nonhuman primates: a functional magnetic resonance imaging study. *Journal of Neuroscience* 24, 2551-2565.
- DeYoe, E.A., Carman, G.J., Bandettini, P., Glickman, S., Wieser, J., Cox, R., Miller, D., and Neitz, J. (1996). Mapping striate and extrastriate visual areas in human cerebral cortex. *Proceedings of the National Academy of Sciences* 93, 2382-2386.
- Dougherty, R.F., Koch, V.M., Brewer, A.A., Fischer, B., Modersitzki, J., and Wandell, B.A. (2003). Visual field representations and locations of visual areas V1/2/3 in human visual cortex. *Journal of vision* 3, 1-1.
- Eickhoff, S.B., Rottschy, C., Kujovic, M., Palomero-Gallagher, N., and Zilles, K. (2008). Organizational principles of human visual cortex revealed by receptor mapping. *Cerebral Cortex* 18, 2637-2645.
- Eickhoff, S.B., Schleicher, A., Scheperjans, F., Palomero-Gallagher, N., and Zilles, K. (2007). Analysis of neurotransmitter receptor distribution patterns in the cerebral cortex. *Neuroimage* 34, 1317-1330.
- Felleman, D.J., and Van Essen, D.C. (1991). Distributed hierarchical processing in the primate cerebral cortex. *Cerebral cortex* 1, 1-47.
- Fize, D., Vanduffel, W., Nelissen, K., Denys, K., d'Hotel, C.C., Faugeras, O., and Orban, G.A. (2003). The retinotopic organization of primate dorsal V4 and surrounding areas: a functional magnetic resonance imaging study in awake monkeys. *Journal of Neuroscience* 23, 7395-7406.
- Gattass, R., Gross, C., and Sandell, J. (1981). Visual topography of V2 in the macaque. *Journal of Comparative Neurology* 201, 519-539.

- Gattass, R., Nascimento-Silva, S., Soares, J.G., Lima, B., Jansen, A.K., Diogo, A.C.M., Farias, M.F., Marcondes, M., Botelho, E.P., Mariani, O.S., *et al.* (2005). Cortical visual areas in monkeys: location, topography, connections, columns, plasticity and cortical dynamics. *Philosophical Transactions of the Royal Society B: Biological Sciences* 360, 709-731.
- Gattass, R., Sousa, A., Mishkin, M., and Ungerleider, L.G. (1997). Cortical projections of area V2 in the macaque. *Cerebral cortex* 7, 110-129.
- Gattass, R., Sousa, A.P., and Gross, C.G. (1988). Visuotopic organization and extent of V3 and V4 of the macaque. *Journal of Neuroscience* 8, 1831-1845.
- Gillen, G. (2015). *Stroke rehabilitation: a function-based approach* (Elsevier Health Sciences).
- Hendry, S., Fuchs, J., DeBlas, A., and Jones, E. (1990). Distribution and plasticity of immunocytochemically localized GABAA receptors in adult monkey visual cortex. *Journal of Neuroscience* 10, 2438-2450.
- Hof, P.R., and Morrison, J.H. (1995). Neurofilament protein defines regional patterns of cortical organization in the macaque monkey visual system: a quantitative immunohistochemical analysis. *Journal of Comparative Neurology* 352, 161-186.
- Horton, J.C., and Hubel, D.H. (1981). Regular patchy distribution of cytochrome oxidase staining in primary visual cortex of macaque monkey. *Nature* 292, 762-764.
- Impieri, D., Zilles, K., Niu, M., Rapan, L., Galletti, C., and Palomero-Gallagher, N. (2018). Receptor architecture of the macaque monkey superior parietal lobule. In 48th Annual Meeting of the Society for Neuroscience (San Diego, USA).
- Kolster, H., Janssens, T., Orban, G.A., and Vanduffel, W. (2014). The retinotopic organization of macaque occipitotemporal cortex anterior to V4 and caudoventral to the middle temporal (MT) cluster. *Journal of Neuroscience* 34, 10168-10191.
- Kötter, R., Stephan, K., Palomero-Gallagher, N., Geyer, S., Schleicher, A., and Zilles, K. (2001). Multimodal characterisation of cortical areas by multivariate analyses of receptor binding and connectivity data. *Anatomy embryology* 204, 333-349.
- Kujovic, M., Zilles, K., Malikovic, A., Schleicher, A., Mohlberg, H., Rottschy, C., Eickhoff, S.B., and Amunts, K. (2013). Cytoarchitectonic mapping of the human dorsal extrastriate cortex. *Brain Structure and Function* 218, 157-172.
- Lerma, J. (2003). Roles and rules of kainate receptors in synaptic transmission. *Nature Reviews Neuroscience* 4, 481-495.
- Lu, H.D., and Roe, A.W. (2008). Functional organization of color domains in V1 and V2 of macaque monkey revealed by optical imaging. *Cerebral Cortex* 18, 516-533.

- Merker, B. (1983). Silver staining of cell bodies by means of physical development. *Journal of neuroscience methods* 9, 235-241.
- Niu, M., Impieri, D., Rapan, L., Funck, T., Palomero-Gallagher, N., and Zilles, K. (2020). Receptor-driven, multimodal mapping of cortical areas in the macaque monkey intraparietal sulcus. *eLife* 9, e55979.
- Niu, M., Rapan, L., Funck, T., Froudast-Walsh, S., Zhao, L., Zilles, K., and Palomero-Gallagher, N. (2021). Organization of the Macaque Monkey Inferior Parietal Lobule Based on Multimodal Receptor Architectonics. *NeuroImage* 231, 117843.
- Olavarria, J.F., and Van Essen, D.C. (1997). The global pattern of cytochrome oxidase stripes in visual area V2 of the macaque monkey. *Cerebral cortex* 7, 395-404.
- Orban, G.A., Fize, D., Peuskens, H., Denys, K., Nelissen, K., Sunaert, S., Todd, J., and Vanduffel, W. (2003). Similarities and differences in motion processing between the human and macaque brain: evidence from fMRI. *Neuropsychologia* 41, 1757-1768.
- Orban, G.A., Van Essen, D., and Vanduffel, W. (2004). Comparative mapping of higher visual areas in monkeys and humans. *Trends Cogn Sci* 8, 315-324.
- Palomero-Gallagher, N., Mohlberg, H., Zilles, K., and Vogt, B. (2008). Cytology and receptor architecture of human anterior cingulate cortex. *Journal of Comparative Neurology* 508, 906-926.
- Palomero-Gallagher, N., Vogt, B.A., Schleicher, A., Mayberg, H.S., and Zilles, K. (2009). Receptor architecture of human cingulate cortex: evaluation of the four-region neurobiological model. *Human brain mapping* 30, 2336-2355.
- Palomero-Gallagher, N., and Zilles, K. (2018). Cyto-and receptor architectonic mapping of the human brain. *Handbook of Clinical Neurology* 150, 355-387.
- Palomero-Gallagher, N., and Zilles, K. (2019). Cortical layers: Cyto-, myelo-, receptor-and synaptic architecture in human cortical areas. *Neuroimage* 197, 716-741.
- Palomero-Gallagher, N., Zilles, K., Schleicher, A., and Vogt, B.A.J.J.o.C.N. (2013). Cyto-and receptor architecture of area 32 in human and macaque brains. *521*, 3272-3286.
- Preuss, T.M., Qi, H., and Kaas, J.H. (1999). Distinctive compartmental organization of human primary visual cortex. *Proceedings of the National Academy of Sciences* 96, 11601-11606.
- Previc, F.H. (1990). Functional specialization in the lower and upper visual fields in humans: Its ecological origins and neurophysiological implications. *Behavioral Brain Sciences* 13, 519-542.
- Rakic, P., Goldman-Rakic, P.S., and Gallager, D. (1988). Quantitative autoradiography of major neurotransmitter receptors in the monkey striate and extrastriate cortex. *Journal of Neuroscience* 8, 3670-3690.
- Rakic, P., and Lidow, M.S. (1995). Distribution and density of monoamine receptors in the primate visual cortex devoid of retinal input from early embryonic stages. *Journal of Neuroscience* 15, 2561-2574.

- Rapan, L., Froudust-Walsh, S., Niu, M., Xu, T., Funck, T., Zilles, K., and Palomero-Gallagher, N. (2021). Multimodal 3D atlas of the macaque monkey motor and premotor cortex. *NeuroImage* 226, 117574.
- Rosa, M.G. (2002). Visual maps in the adult primate cerebral cortex: some implications for brain development and evolution. *Brazilian Journal of Medical Biological Research* 35, 1485-1498.
- Rosa, M.G., Palmer, S.M., Gamberini, M., Tweedale, R., Piñon, M.C., and Bourne, J.A. (2005). Resolving the organization of the New World monkey third visual complex: the dorsal extrastriate cortex of the marmoset (*Callithrix jacchus*). *Journal of Comparative Neurology* 483, 164-191.
- Rosier, A.-M., Arckens, L., Orban, G., and Vandesande, F. (1993). Laminar distribution of NMDA receptors in cat and monkey visual cortex visualized by [3H]-MK-801 binding. *Journal of Comparative Neurology* 335, 369-380.
- Rosier, A.-M., Leroux, P., Vaudry, H., Orban, G., and Vandesande, F. (1991). Distribution of somatostatin receptors in the cat and monkey visual cortex demonstrated by in vitro receptor autoradiography. *Journal of Comparative Neurology* 310, 189-199.
- Rottschy, C., Eickhoff, S.B., Schleicher, A., Mohlberg, H., Kujovic, M., Zilles, K., and Amunts, K. (2007). Ventral visual cortex in humans: cytoarchitectonic mapping of two extrastriate areas. *Human brain mapping* 28, 1045-1059.
- Rousseeuw, P. (1987). Silhouettes: a graphical aid to the interpretation and validation of cluster analysis. *Journal of computational applied mathematics* 20, 53-65.
- Schira, M.M., Tyler, C.W., and Rosa, M.G. (2012). Brain mapping: the (un) folding of striate cortex. *Current Biology* 22, R1051-R1053.
- Sereno, M.I., Dale, A., Reppas, J., Kwong, K., Belliveau, J., Brady, T., Rosen, B., and Tootell, R. (1995). Borders of multiple visual areas in humans revealed by functional magnetic resonance imaging. *Science* 268, 889-893.
- Sherwood, C.C., Holloway, R.L., Erwin, J.M., and Hof, P.R. (2004). Cortical orofacial motor representation in old world monkeys, great apes, and humans. *Brain, behavior and evolution* 63, 82-106.
- Silson, E.H., Reynolds, R.C., Kravitz, D.J., and Baker, C.I. (2018). Differential sampling of visual space in ventral and dorsal early visual cortex. *Journal of Neuroscience* 38, 2294-2303.
- Takemura, H., Palomero-Gallagher, N., Axer, M., Gräbel, D., Jorgensen, M.J., Woods, R., and Zilles, K. (2020). Anatomy of nerve fiber bundles at micrometer-resolution in the vervet monkey visual system. *elife* 9, e55444.
- Team, R.C. (2013). R: A language and environment for statistical computing.

- Tolias, A.S., Smirnakis, S.M., Augath, M.A., Trinath, T., and Logothetis, N.K. (2001). Motion processing in the macaque: revisited with functional magnetic resonance imaging. *Journal of Neuroscience* 21, 8594-8601.
- Tootell, R.B., Dale, A.M., Sereno, M.I., and Malach, R. (1996). New images from human visual cortex. *Trends in neurosciences* 19, 481-489.
- Tootell, R.B., Mendola, J.D., Hadjikhani, N.K., Ledden, P.J., Liu, A.K., Reppas, J.B., Sereno, M.I., and Dale, A.M. (1997). Functional analysis of V3A and related areas in human visual cortex. *Journal of Neuroscience* 17, 7060-7078.
- Tsao, D.Y., Freiwald, W.A., Knutsen, T.A., Mandeville, J.B., and Tootell, R.B. (2003). Faces and objects in macaque cerebral cortex. *Nature neuroscience* 6, 989-995.
- Ungerleider, L.G. (1982). Two cortical visual systems. *Analysis of visual behavior*, 549-586.
- Ungerleider, L.G., Galkin, T.W., Desimone, R., and Gattass, R. (2008). Cortical connections of area V4 in the macaque. *Cerebral Cortex* 18, 477-499.
- Van Essen, D., Newsome, W., Maunsell, J., and Bixby, J. (1986). The projections from striate cortex (V1) to areas V2 and V3 in the macaque monkey: asymmetries, areal boundaries, and patchy connections. *Journal of Comparative Neurology* 244, 451-480.
- Van Essen, D.C. (2003). Organization of visual areas in macaque and human cerebral cortex. *The visual neurosciences* 1, 507-521.
- Van Polanen, V., and Davare, M. (2015). Interactions between dorsal and ventral streams for controlling skilled grasp. *Neuropsychologia* 79, 186-191.
- Vanduffel, W., Fize, D., Mandeville, J.B., Nelissen, K., Van Hecke, P., Rosen, B.R., Tootell, R.B., and Orban, G.A. (2001). Visual motion processing investigated using contrast agent-enhanced fMRI in awake behaving monkeys. *Neuron* 32, 565-577.
- Vanduffel, W., Fize, D., Peuskens, H., Denys, K., Sunaert, S., Todd, J., and Orban, G. (2002). Extracting 3D from motion: differences in human and monkey intraparietal cortex. *Science* 298, 413-415.
- Wilms, M., Eickhoff, S.B., Hömke, L., Rottschy, C., Kujovic, M., Amunts, K., and Fink, G.R. (2010). Comparison of functional and cytoarchitectonic maps of human visual areas V1, V2, V3d, V3v, and V4 (v). *Neuroimage* 49, 1171-1179.
- Wong-Riley, M. (1979). Changes in the visual system of monocularly sutured or enucleated cats demonstrable with cytochrome oxidase histochemistry. *Brain research* 171, 11-28.
- Zeki, S. (1978). The third visual complex of rhesus monkey prestriate cortex. *The Journal of Physiology* 277, 245-272.

- Zhu, Q., and Vanduffel, W. (2019). Submillimeter fMRI reveals a layout of dorsal visual cortex in macaques, remarkably similar to New World monkeys. *Proceedings of the National Academy of Sciences* *116*, 2306-2311.
- Zilles, K., Bacha-Trams, M., Palomero-Gallagher, N., Amunts, K., and Friederici, A.D. (2015a). Common molecular basis of the sentence comprehension network revealed by neurotransmitter receptor fingerprints. *Cortex* *63*, 79-89.
- Zilles, K., and Clarke, S. (1997). Architecture, connectivity, and transmitter receptors of human extrastriate visual cortex. In *Extrastriate cortex in primates* (Springer), pp. 673-742.
- Zilles, K., and Palomero-Gallagher, N. (2017a). Comparative analysis of receptor types that identify primary cortical sensory areas. In *Evolution of Nervous Systems*, 2nd Edition, K. JH, ed. (Elsevier), pp. 225-245.
- Zilles, K., and Palomero-Gallagher, N. (2017b). Multiple transmitter receptors in regions and layers of the human cerebral cortex. *Frontiers in neuroanatomy* *11*, 78.
- Zilles, K., Palomero-Gallagher, N., Bludau S, Mohlberg H, and Amunts, K. (2015b). Cytoarchitecture and Maps of the Human Cerebral Cortex In: *Brain Mapping*. In (San Diego: Elsevier Academic), pp. 115-135.
- Zilles, K., and Schleicher, A. (1993). Cyto- and myeloarchitecture of human visual cortex and the periodical GABAA receptor distribution. In *Functional organisation of the human visual cortex* (Elsevier), pp. 111-122.
- Zilles, K., Schleicher, A., Palomero-Gallagher, N., and Amunts, K. (2002). Quantitative analysis of cyto- and receptor architecture of the human brain. In *Brain mapping: the methods*, pp. 573-602.

Figure Captions

Figure 1. Topography of the eight cyto- and receptor architectonically distinct areas identified in the macaque brain depicted on the Yerkes 19 surface. (map made publicly available at <https://balsa.wustl.edu/study/l77k6>) Abbreviations: *cas* calcarine sulcus, *pos* parieto-occipital sulcus, *ots* occipito-temporal sulcus, *lus* lunate sulcus, *ios* inferior occipital sulcus.

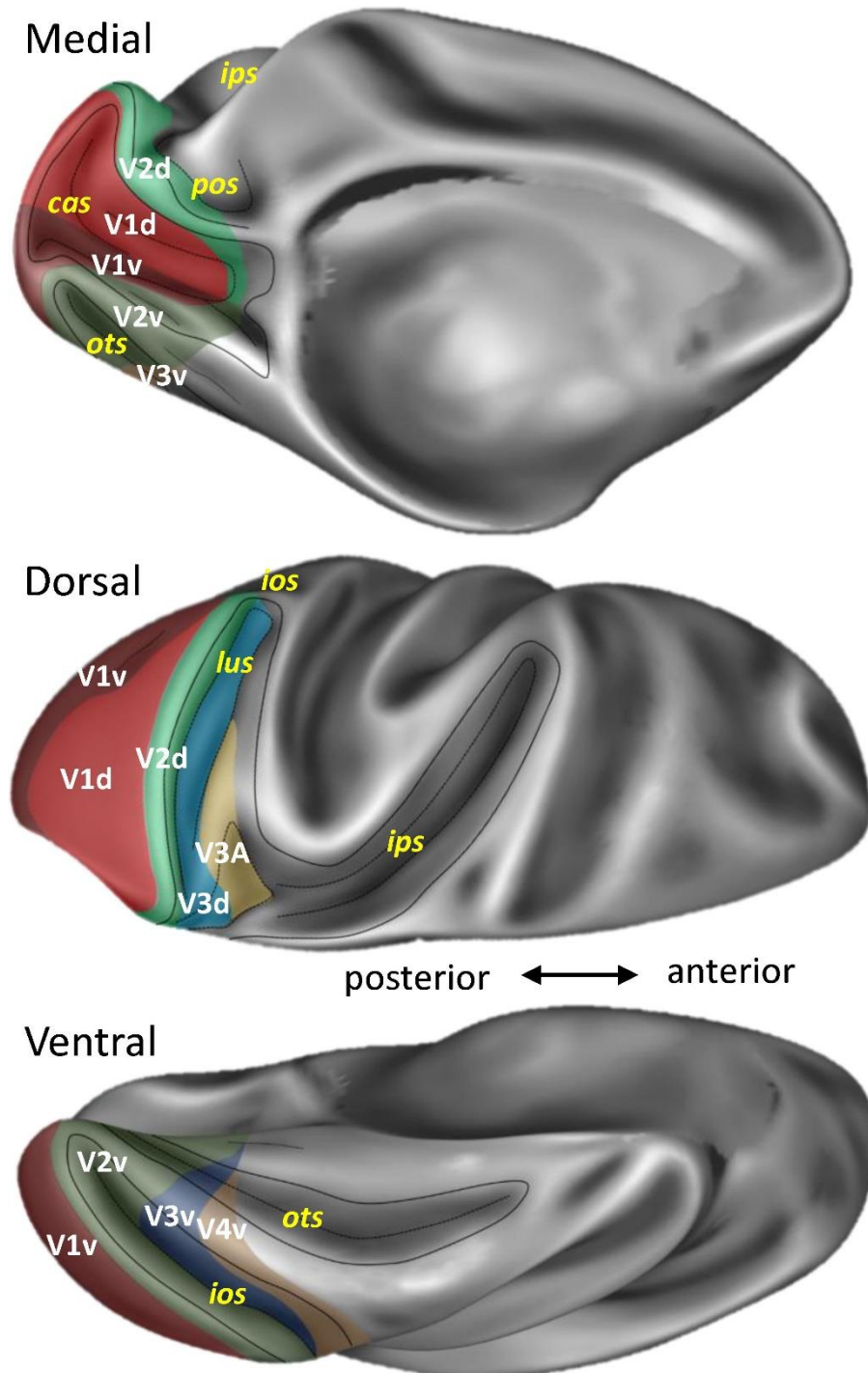
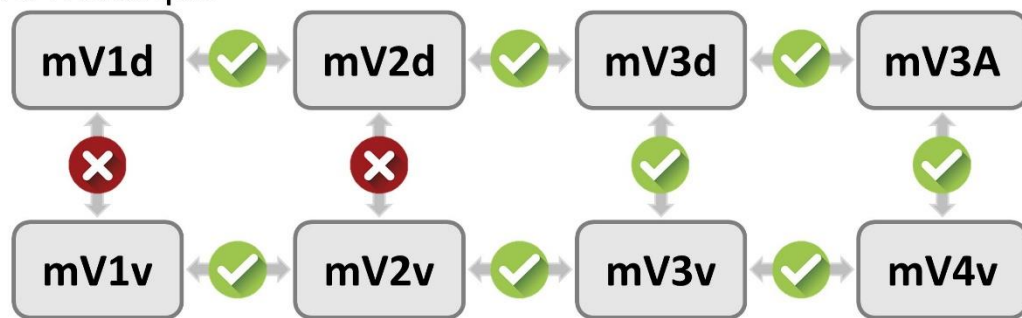


Figure 2. Schematic representation of the strategy used for statistical testing of differences in mean receptor densities between early visual areas. For each species, the statistical testing process involved three steps. 1) an omnibus test was carried out to determine whether there were differences across all areas when all receptor types are considered simultaneously. 2) The simple effect tests were performed for each receptor separately to determine if this receptor type contributed to the distinction of early visual areas. 3) For those receptor types that were found to show significant differences across all areas in the second step tests, post hoc tests were used to explore which paired areas drive the statistical difference. Arrows indicate pairs of areas compared. Results of the statistical analysis (after correction of p-values) are indicated by checkmarks in green circles (significant finding) or crosses in red circles (the two areas do not differ significantly in their receptor architecture). For information concerning which receptor types contributed to the significance, see [Supplementary Fig. 5](#). Statistical values for the first level test are provided in [Supplementary table 2](#), those of the simple effects in [Supplementary table 2](#), and those of post-hoc tests in [Supplementary tables 4 and 5](#) (macaque and human data, respectively).

A. Macaque



B. Human

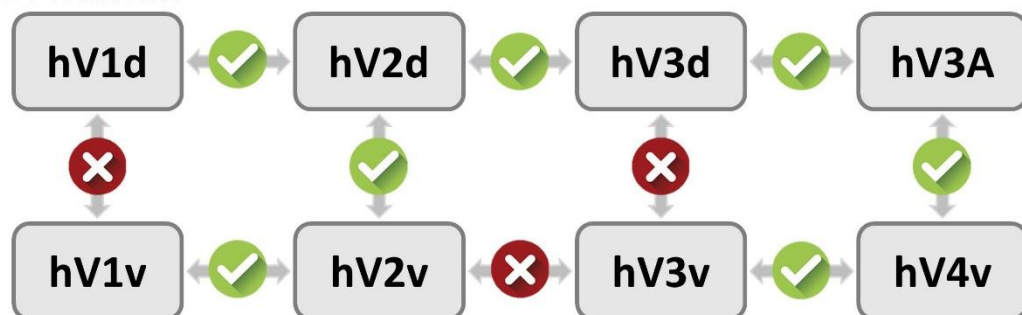


Figure 3. Cyto- and receptor architecture of macaque primary visual area V1. **A:** Schematic drawing of a coronal section through the macaque brain showing the position of dorsal (mV1d) and ventral (mV1v) subdivisions of V1 within the calcarine sulcus. **B:** High-resolution photomicrographs of cytoarchitectonic features of areas mV1d and mV1v. Scale bar 300 μ m. Roman numerals indicate cytoarchitectonic layers. **C:** Exemplary sections depicting the distribution of kainate, NMDA, GABA_A, GABA_B, M₂, M₃, 5-HT_{1A} and 5-HT₂ receptors. The color bar next to each autoradiograph codes for receptor density in fmol/mg protein and borders are indicated by the white lines. Distribution patterns of the remaining receptors are shown in [Supplementary Fig. 1](#). For abbreviations see [Fig. 1](#).

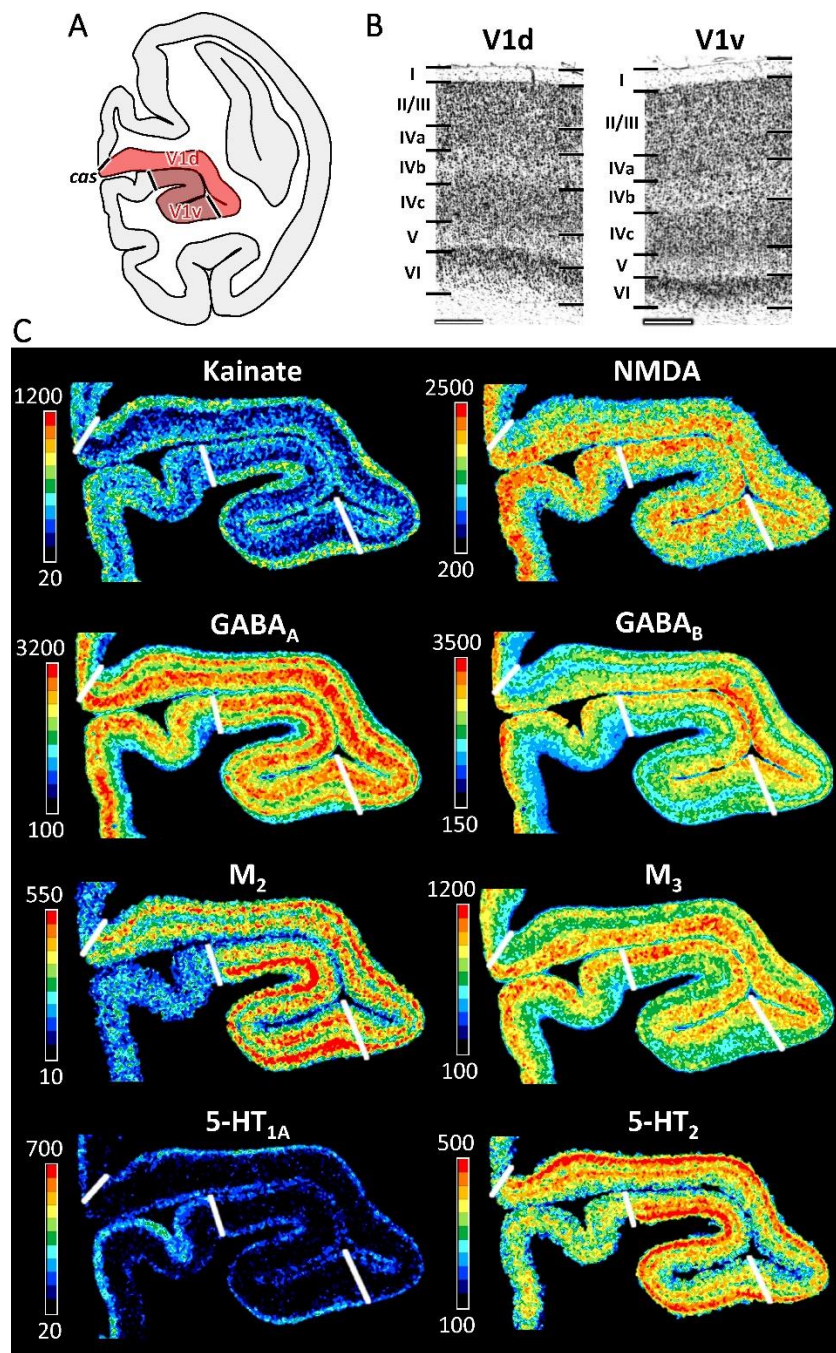


Figure 4. Cyto- and receptor architecture of macaque ventral early extrastriate visual areas. **A:** Schematic drawing of a coronal section through the macaque brain showing the position of areas mV2v, mV3v and mV4v. **B:** High-resolution photomicrographs of cytoarchitectonic features of areas mV2v, mV3v and mV4v. Scale bar 300 μ m. Roman numerals indicate cytoarchitectonic layers. **C:** Exemplary sections depicting the distribution of AMPA, kainate, NMDA, GABA_B, M₂ and 5-HT_{1A} receptors. The color bar next to each autoradiograph codes for receptor density in fmol/mg protein and borders are indicated by the white lines. Distribution patterns of the remaining receptors are shown in [Supplementary Fig. 2](#). For abbreviations see [Fig. 1](#).

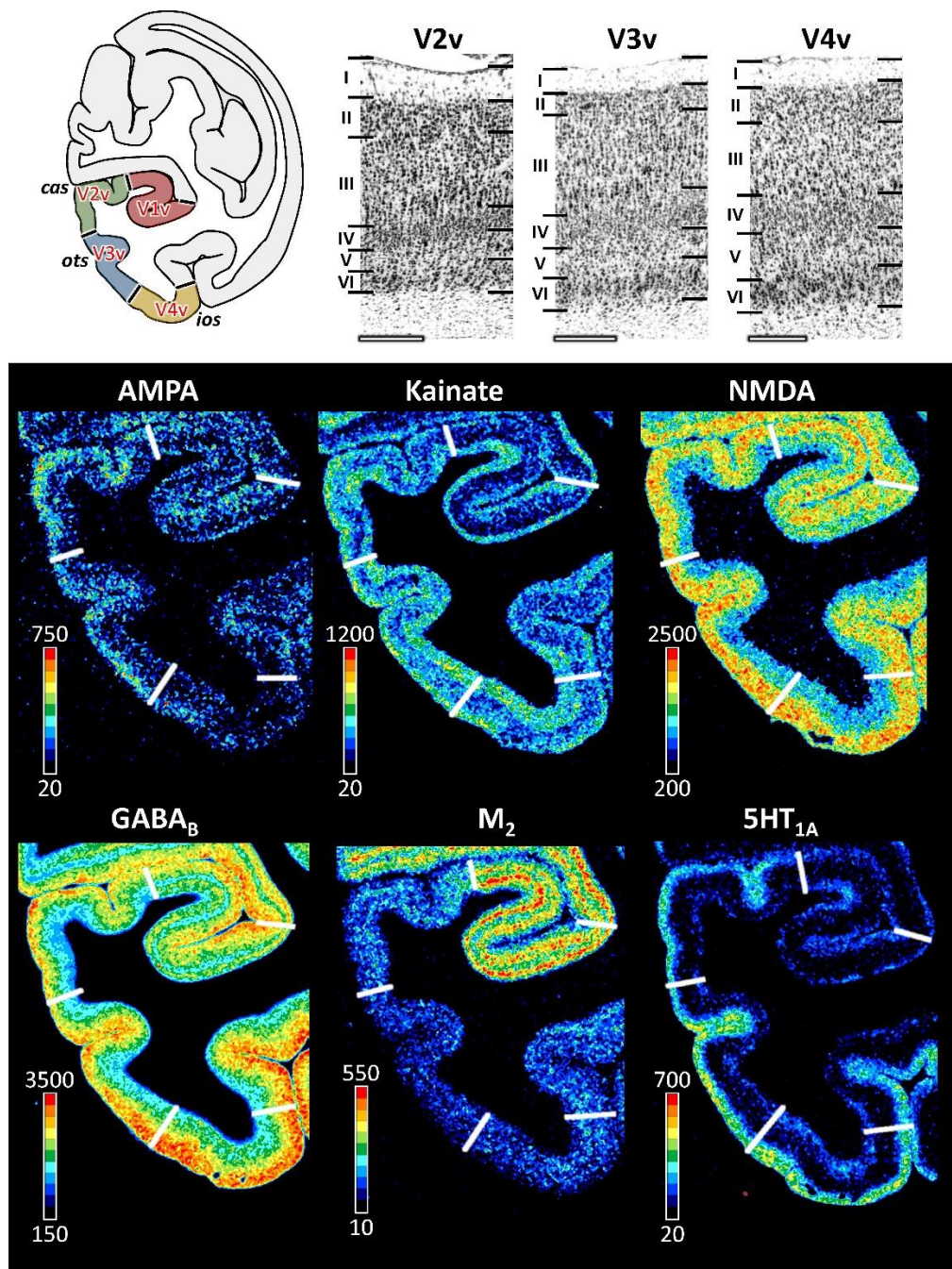


Figure 5. Cyto- and receptor architecture of macaque dorsal early extrastriate visual areas. **A:** Schematic drawing of a coronal section through the macaque brain showing the position of areas mV2d, mV3d and mV3A. **B:** High-resolution photomicrographs of cytoarchitectonic features of areas mV2d, mV3d and mV3A. Scale bar 300 μ m. Roman numerals indicate cytoarchitectonic layers. **C:** Exemplary sections depicting the distribution of kainate, GABA_A, GABA_B and α_1 receptors. The color bar next to each autoradiograph codes for receptor density in fmol/mg protein and borders are indicated by the white lines. Distribution patterns of the remaining receptors are shown in [Supplementary Fig. 3](#). For abbreviations see [Fig. 1](#).

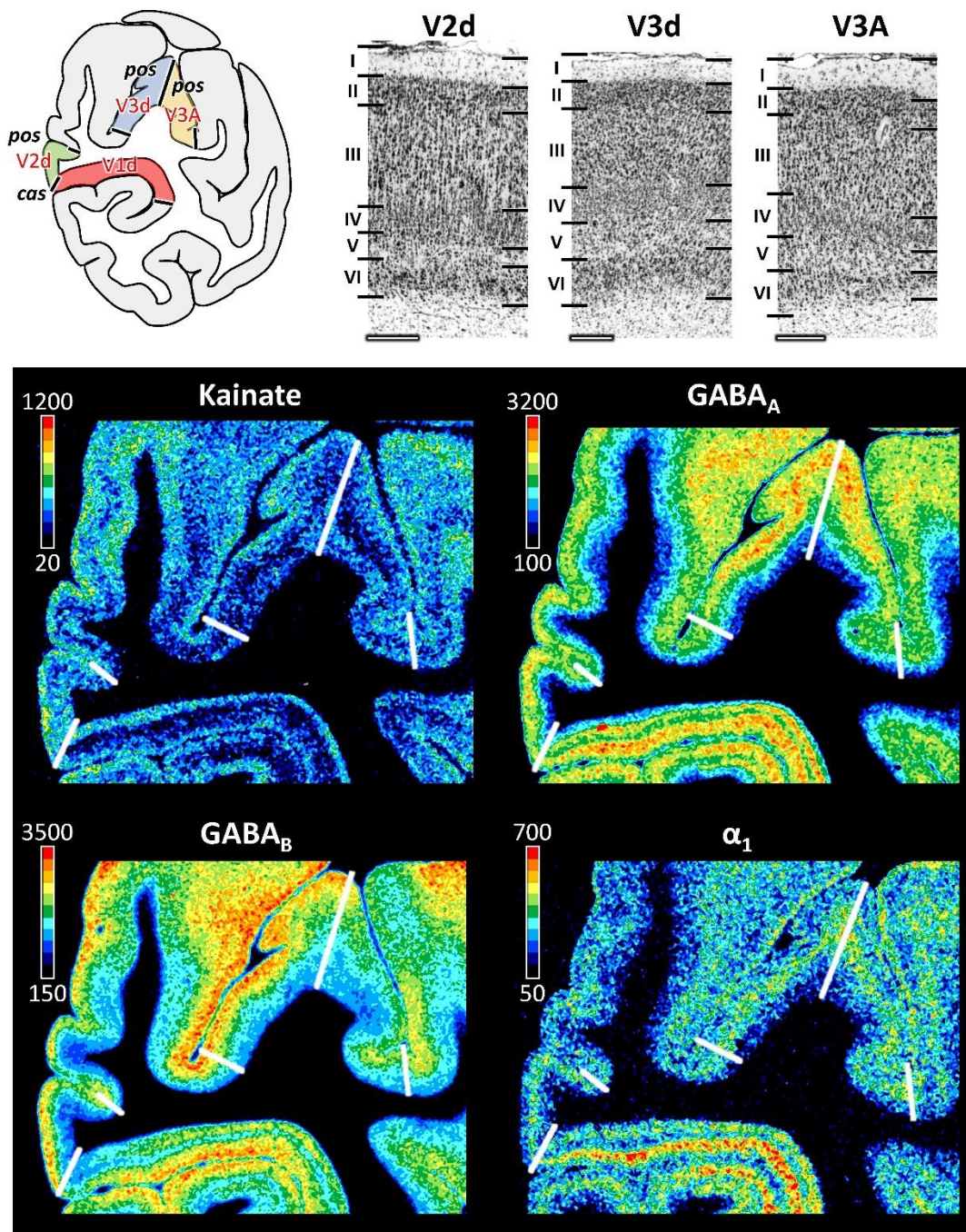


Figure 6. Receptor fingerprints of the early visual areas in the macaque monkey and human brain. Absolute receptor densities are given in fmol/mg protein. The positions of the different receptor types and the axis scaling are identical in all areas, and specified in the polar plot in the middle of the figure. Data is publicly available via the EBRAINS platform of the Human Brain Project (<https://search.kg.ebrains.eu/instances/Project/e39a0407-a98a-480e-9c63-4a2225ddfbe4>) and under <https://balsa.wustl.edu/study/l77k6>.

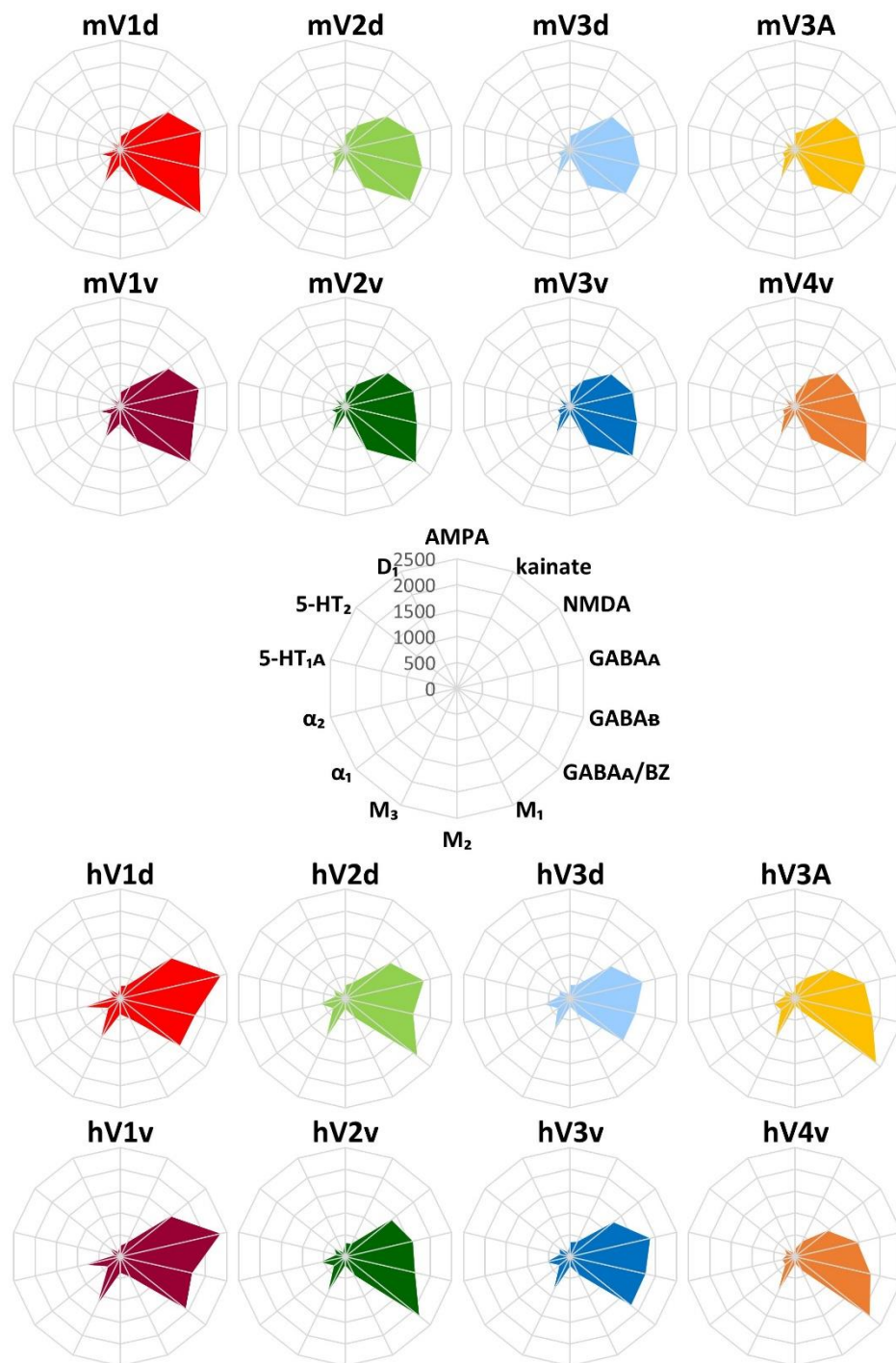
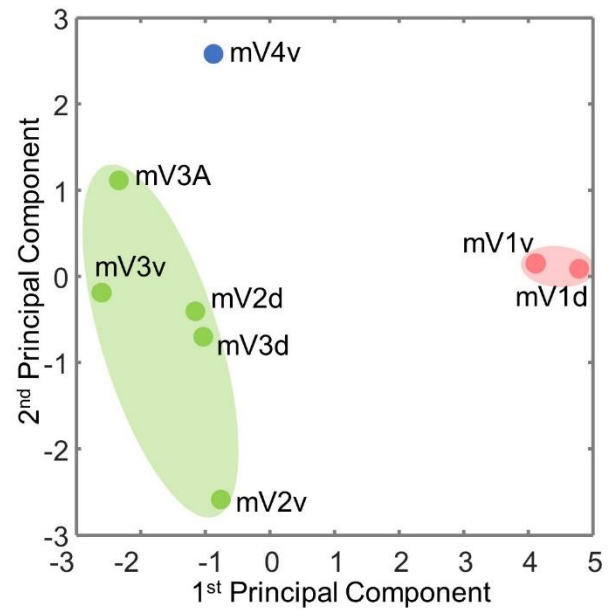
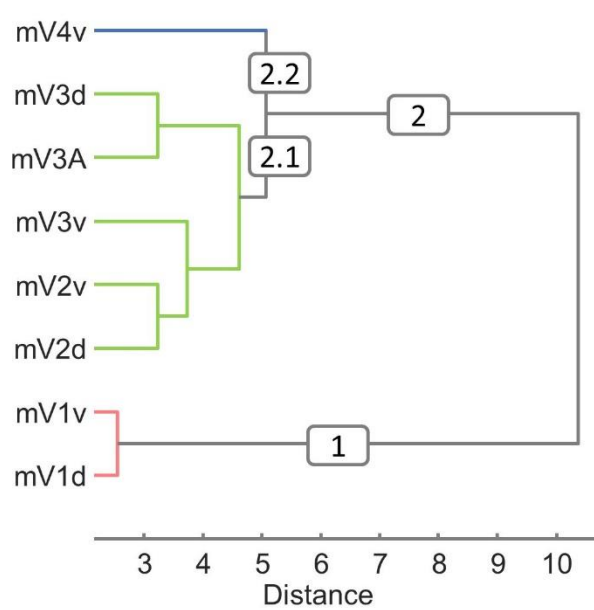


Figure 7. Hierarchical clustering and principal component analysis (PCA) aiming to determine clustering of visual areas based on (dis)similarities in their normalized receptor fingerprints. *k*-means clustering and elbow analysis showed three as the optimal number of clusters for both species. **A:** Macaque monkey visual areas **B:** Human visual areas. Receptor densities were normalized separately for macaque and human visual areas, and data is provided in [Supplementary table 7](#).

A Macaque



B Human

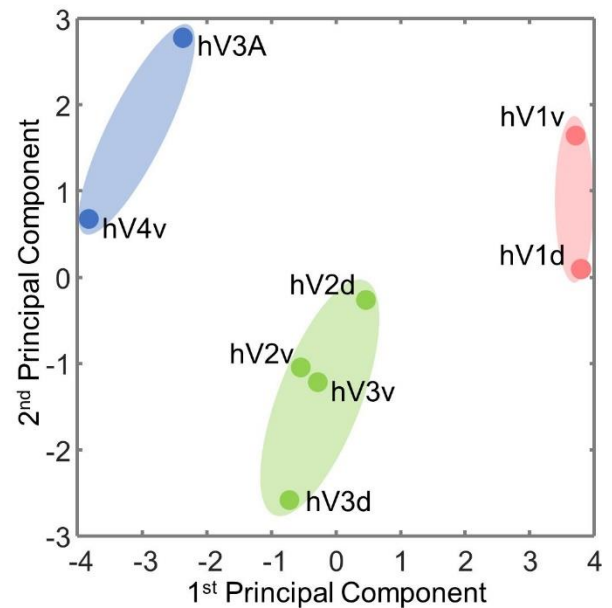
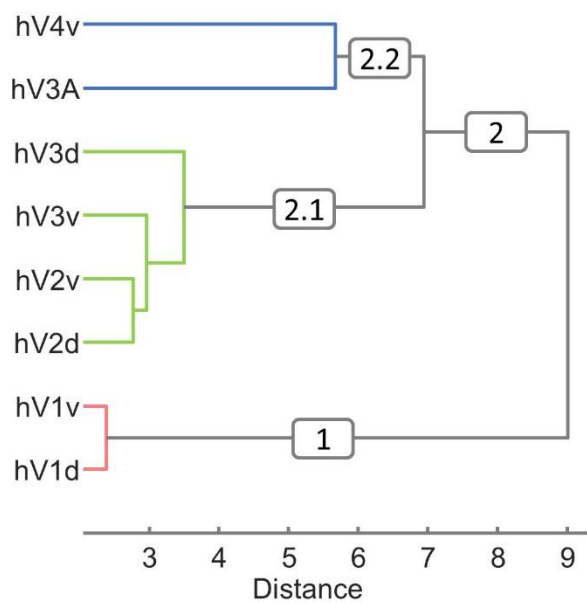
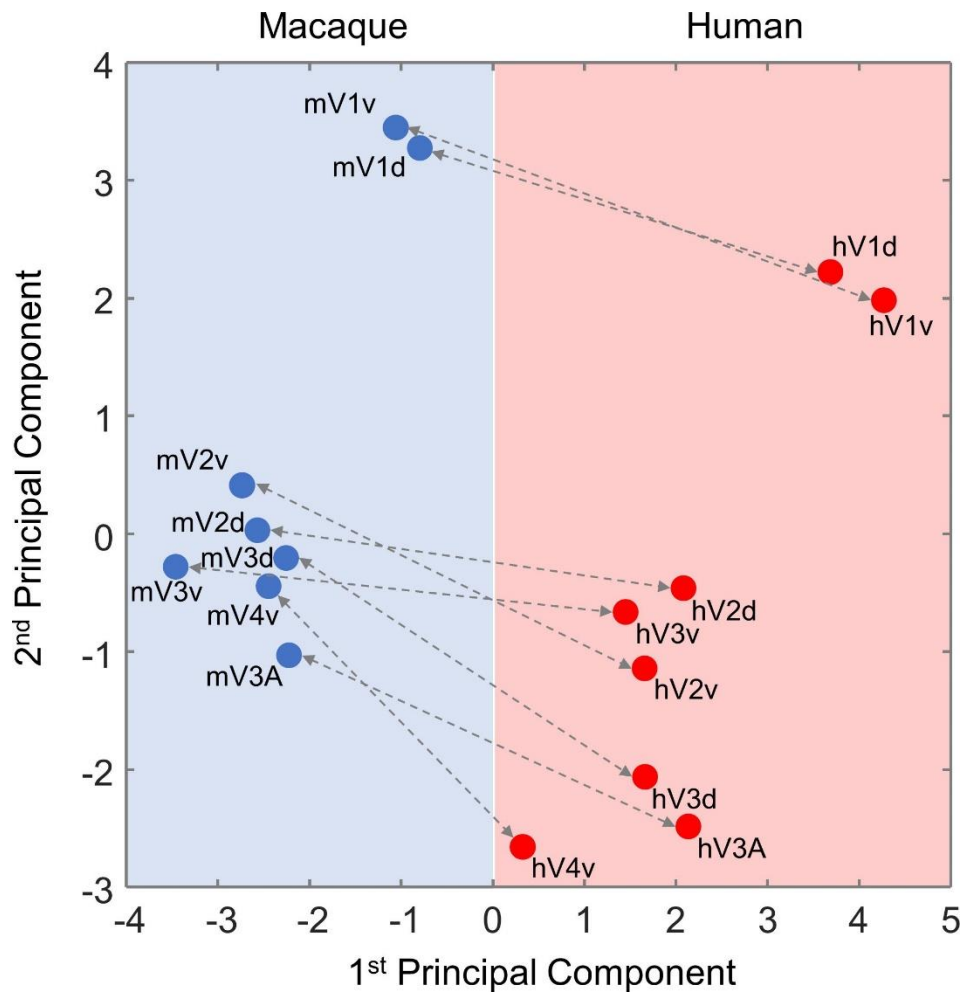
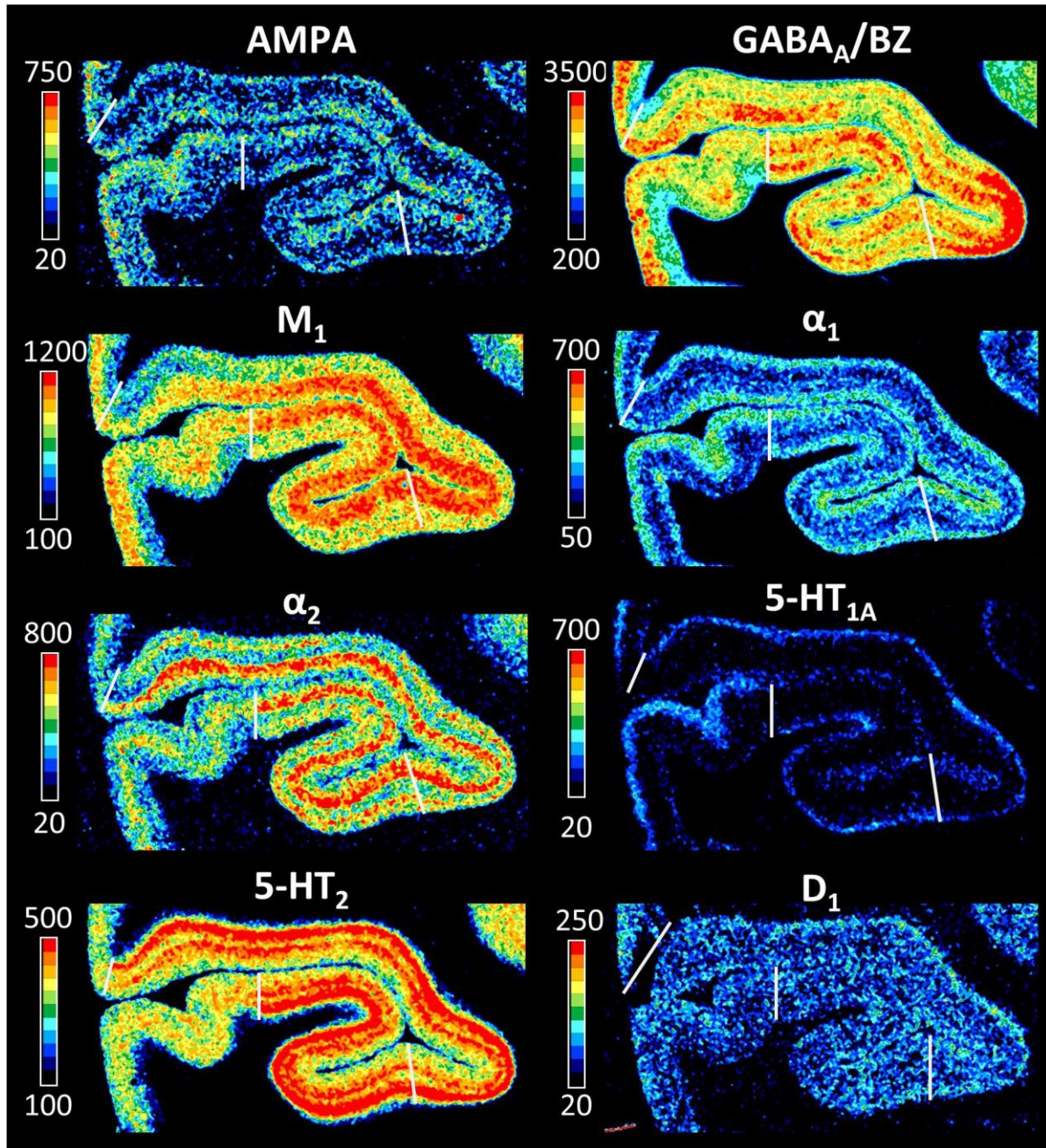


Figure 8. A species-combined principal component analysis (PCA) of the receptor densities in human (red) and macaque (blue) primary and early extrastriate visual areas. Receptor densities were normalized after combining both species into the same space, and data is provided in [Supplementary table 8](#).

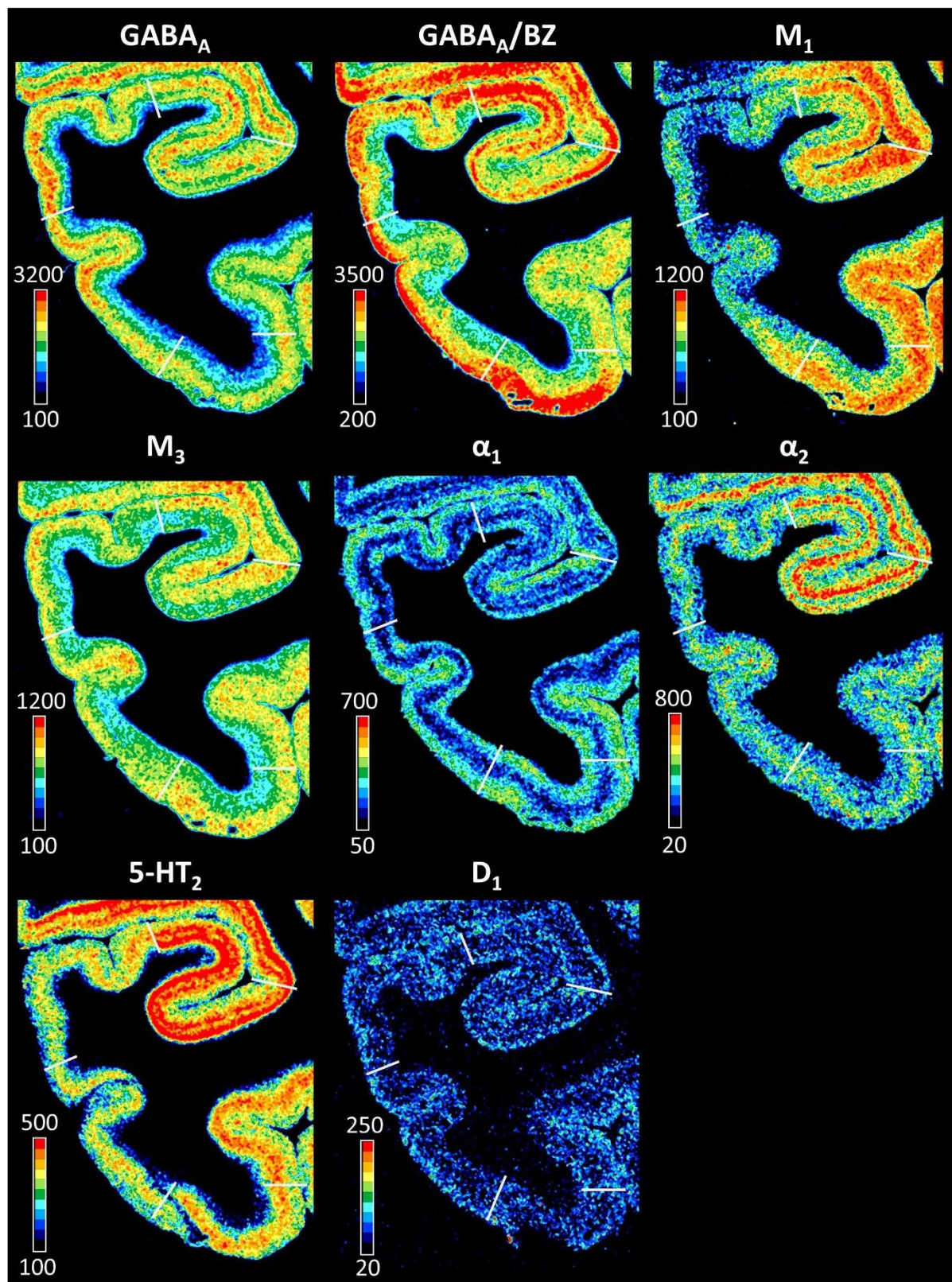


Supplementary material

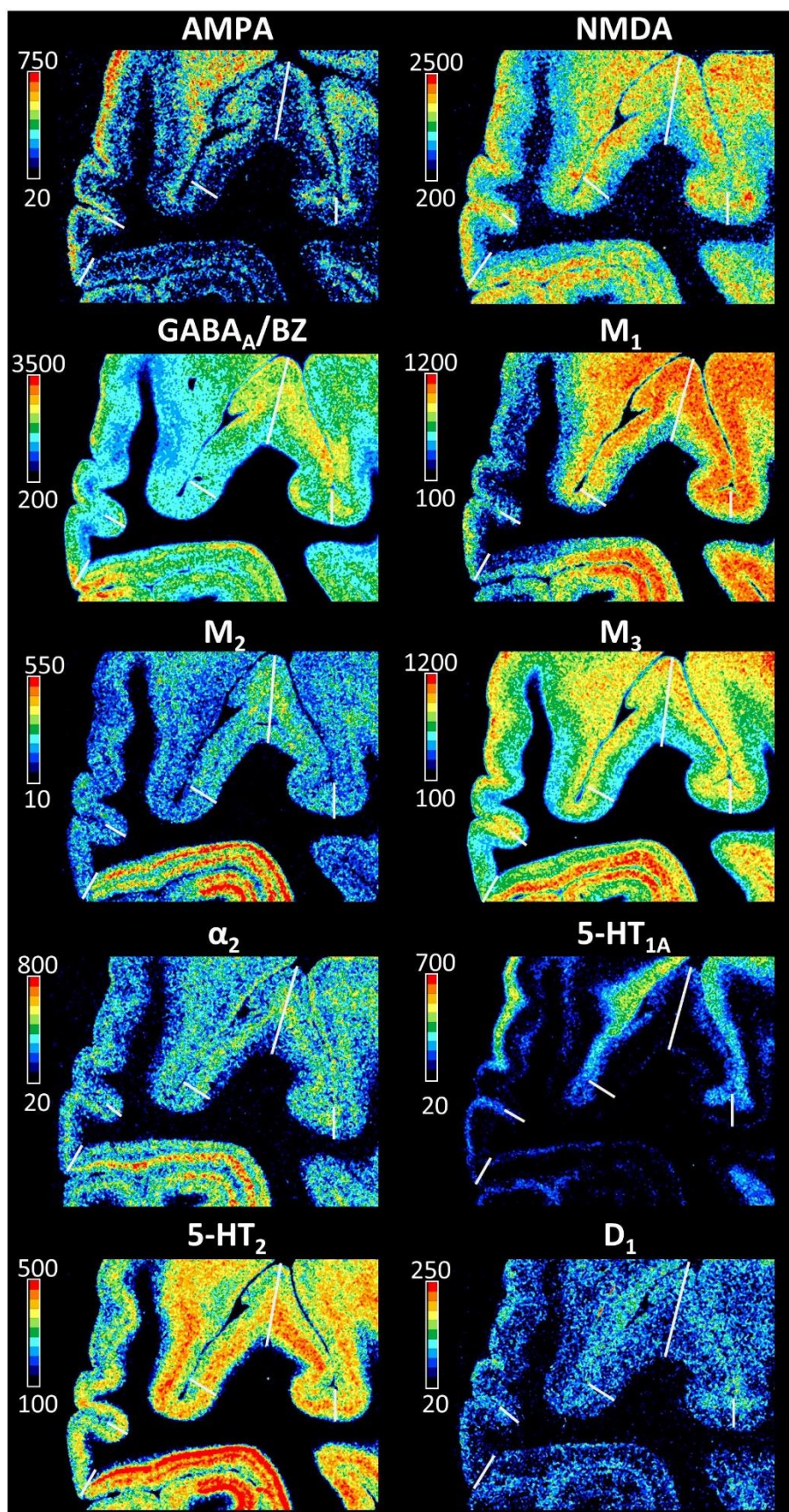
Supplementary Figure 1. Receptor architecture of macaque primary visual area V1. For details see [Fig. 3](#).



Supplementary Figure 2. Receptor architecture of macaque ventral visual areas. For details see Fig. 4.

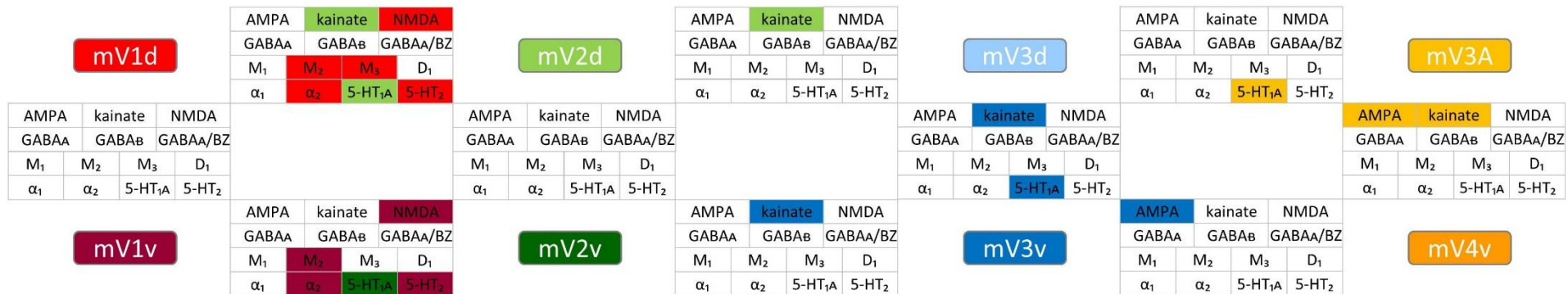


Supplementary Figure 3. Receptor architecture of macaque dorsal visual areas. For details see Fig. 5.

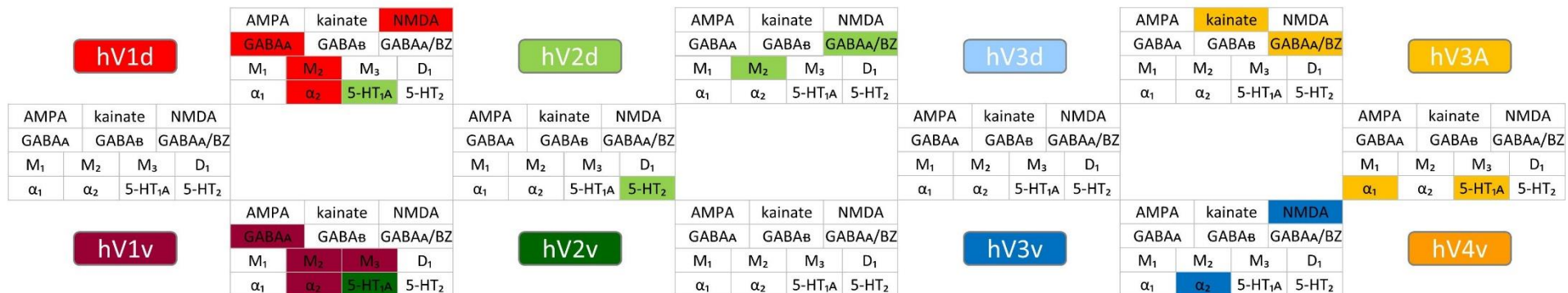


Supplementary Figure 4. Schematic representation of the result of the statistical analysis of interareal differences in receptor densities. The receptors highlighted by a coloured background were found to differ significantly between the corresponding pairs of areas, and colour used indicates area with the highest density for that receptor. For details on the statistical strategy see Figure 2, and for statistical values for each level test, see Supplementary Tables 2-5.

A. Macaque



B. Human



Supplementary Figure 5. Schematic representation of the interareal differences in receptor densities between V3v and V3A, as well as those between V3d and V4v. Areas V3v and V3A differed significantly in both the macaque and the human brain. Macaque mV3v contains higher kainate receptor densities than does mV3A. Human hV3v contains higher NMDA and M₁ but lower kainate and GABA_A/BZ receptor densities than does hV3A. Areas V3d and V4v differed significantly in both the macaque and the human brain. Macaque mV3d contains lower kainate receptor densities than does mV4v. Human hV3d contains higher NMDA, α_1 and 5-HT_{1A} but lower GABA_A/BZ receptor densities than does hV4v. For details on the statistical strategy see Figure 2, and for statistical values for each level test, see Supplementary Tables 2-5.

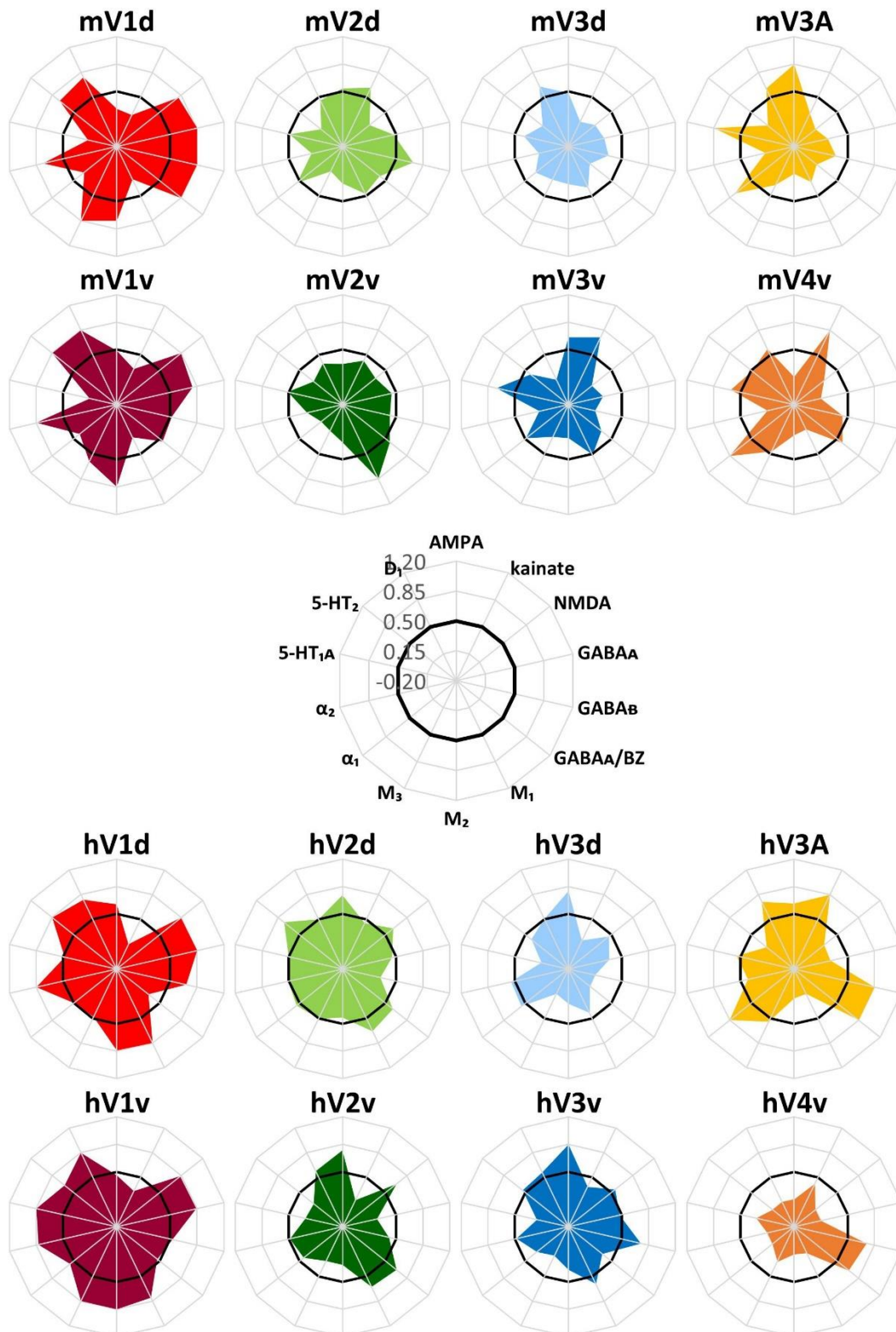
A. Macaque

mV3v				VS	mV3A			
AMPA	kainate	NMDA			AMPA	kainate	NMDA	
GABA _A	GABA _B	GABA _A /BZ			GABA _A	GABA _B	GABA _A /BZ	
M ₁	M ₂	M ₃	D ₁		M ₁	M ₂	M ₃	D ₁
α_1	α_2	5-HT _{1A}	5-HT ₂		α_1	α_2	5-HT _{1A}	5-HT ₂

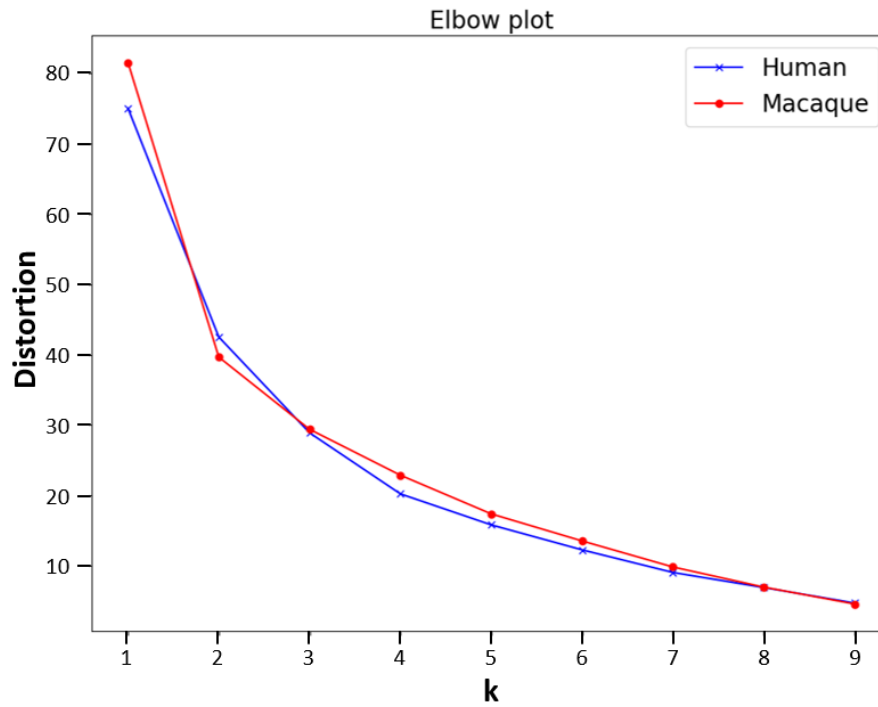
B. Human

hV3v				VS	hV3A			
AMPA	kainate	NMDA			AMPA	kainate	NMDA	
GABA _A	GABA _B	GABA _A /BZ			GABA _A	GABA _B	GABA _A /BZ	
M ₁	M ₂	M ₃	D ₁		M ₁	M ₂	M ₃	D ₁
α_1	α_2	5-HT _{1A}	5-HT ₂		α_1	α_2	5-HT _{1A}	5-HT ₂

Supplementary Figure 6. Normalized receptor fingerprints of the early visual areas in the macaque monkey and human brain. The receptor fingerprints were normalized by min-max scaling, and the thick black line in each plot indicates the average normalized value over all areas. The positions of the different receptor types and the axis scaling (-1.0/+1.0) are identical in all areas, and specified in the polar plot in the middle of the figure.

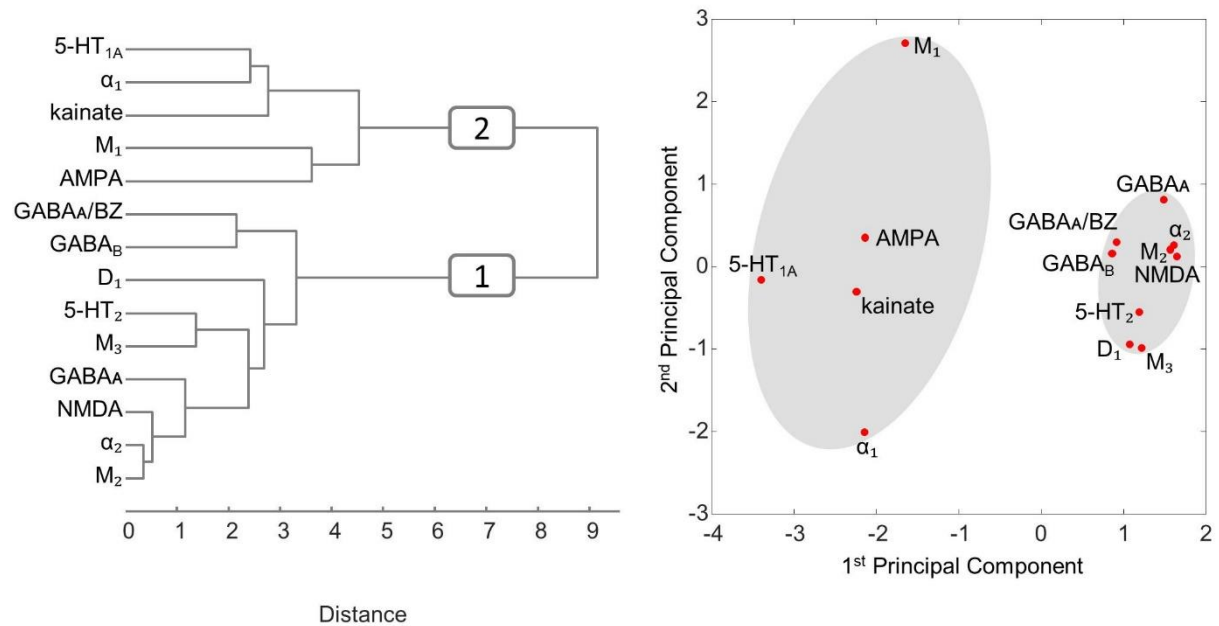


Supplementary Figure 7. Elbow plot of the K means analyses aiming to determine the number of stable clusters of areas of the macaque (red) and human (blue) brains based on (dis)similarities in their normalized receptor fingerprints.

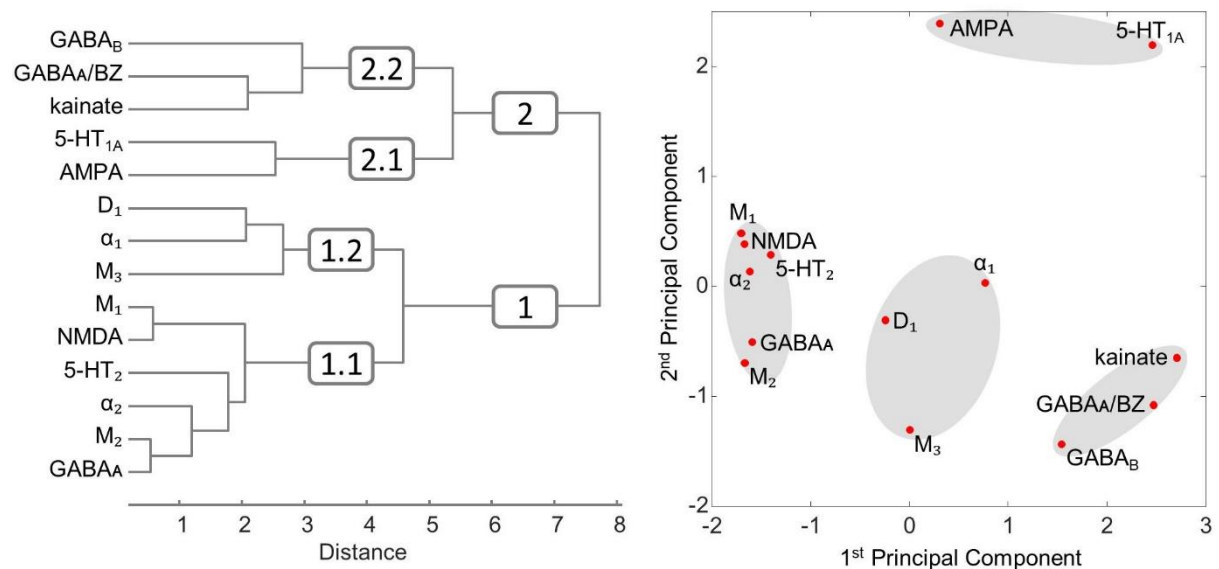


Supplementary Figure 8. Hierarchical clustering and principal component analysis (PCA) aiming to determine clustering of receptor types based on (dis)similarities in the changes of their densities across visual areas. **A:** Macaque monkey visual areas **B:** Human visual areas. Receptor densities were normalized separately for macaque and human visual areas, and analyses were carried out with a transposed version of the data provided in [Supplementary table 7](#).

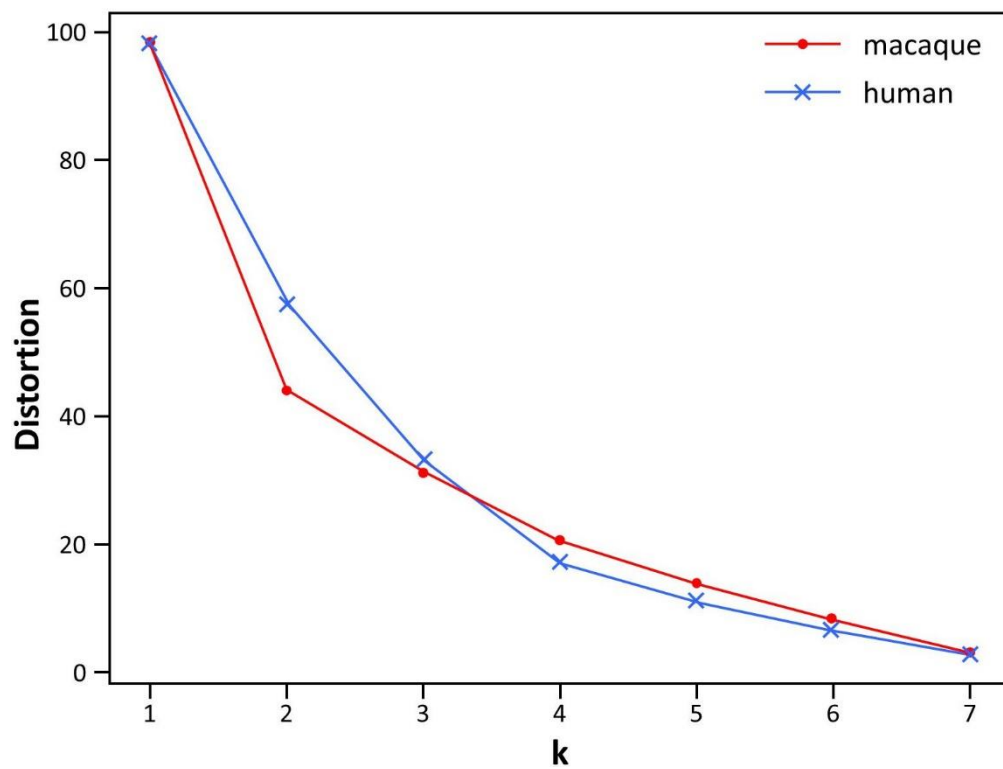
A Macaque



B Human



Supplementary Figure 9. Elbow plot of the K means analyses aiming to determine the number of stable clusters of receptor types based on (dis)similarities of their expression levels throughout macaque (red) and human (blue) visual areas.



Supplementary Table 1. Incubation protocols

Transmitter	Receptor	Ligand (nM)	Displacer	Incubation buffer	Pre-incubation	Main incubation	Final rinsing
Glutamate	AMPA	[³ H]-AMPA (10.0)	Quisqualate (10 µM)	50 mM Tris-acetate (pH 7.2) [+ 100 mM KSCN]*	3x10 min, 4°C	45 min, 4°C	1) 4x4 sec 2) Acetone/glutaraldehyde (100 ml + 2,5 ml), 2x2 sec,
	NMDA	[³ H]-MK801 (3.3)	(+)-MK-801 (100 µM)	50 mM Tris-acetate (pH 7.2) + 50 µM glutamate [+ 30 µM glycine + 50 µM	15 min, 4°C	60 min, 22°C	1) 2x5 min, 4°C 2) Distilled water, 1x22°C
	Kainate	[³ H]-Kainate (9.4)	SYM 2081 (100 µM)	50 mM Tris-acetate (pH 7.2) [+ 10 mM Ca ²⁺ -acetate]*	3x10 min, 4°C	45 min, 4°C	1) 3x4 sec 2) Acetone/glutaraldehyde (100 ml + 2,5 ml), 2x2 sec,
GABA	GABA _A	[³ H]-Muscimol (7.7)	GABA (10 µM)	50 mM Tris-citrate (pH 7.0)	3x5 min, 4°C	40 min, 4°C	1) 3x3 sec, 4°C 2) Distilled water, 1x22°C
	GABA _B	[³ H]-CGP 54626	CGP 55845 (100 µM)	50 mM Tris-HCl (pH 7.2) + 2.5 mM CaCl ₂	3x5 min, 4°C	60 min, 4°C	1) 3x2 sec, 4°C 2) Distilled water, 1x22°C
	GABA _A /BZ	[³ H]-Flumazenil (1.0)	Clonazepam (2 µM)	170 mM Tris-HCl (pH 7.4)	15 min, 4°C	60 min, 4°C	1) 2x1 min, 4°C 2) Distilled water, 1x22°C
Acetylcholine	M ₁	[³ H]-Pirenzepine	Pirenzepine (2 µM)	Modified Krebs buffer (pH 7.4)	15 min, 4°C	60 min, 4°C	1) 2x1 min, 4°C 2) Distilled water, 1x22°C
	M ₂	[³ H]-Oxotremorine-	Carbacol (10 µM)	20 mM HEPES-Tris (pH 7.5) + 10 mM MgCl ₂ + 300 nM Pirenzepine	20 min, 22°C	60 min, 22°C	1) 2x2 min, 4°C 2) Distilled water, 1x22°C
	M ₃	[³ H]-4-DAMP (1.0)	Atropine sulfate (10 µM)	50 mM Tris-HCl (pH 7.4) + 0.1 mM PSMF + 1mM EDTA	15 min, 22° C	45 min, 22° C	1) 2x5 min, 4° C 2) distilled water, 1x22°C
Noradrenaline	α ₁	[³ H]-Prazosin (0.2)	Phentolamine Mesylate	50 mM Na/K-phosphate buffer (pH 7.4)	15 min, 22°C	60 min, 22°C	1) 2x5 min, 4°C 2) Distilled water, 1x22°C
	α ₂	[³ H]-UK 14,304 (0,64)	Phentolamine Mesylate	50 mM Tris-HCl + 100 µM MnCl ₂ (pH 7.7)	15 min, 22°C	90 min, 22°C	1) 5 min, 4°C 2) Distilled water, 1x22°C
Serotonin	5-HT _{1A}	[³ H]-8-OH-DPAT	5-Hydroxy-tryptamine	170 mM Tris-HCl (pH 7.4) [+ 4 mM CaCl ₂ + 0.01% ascorbate]*	30 min, 22°C	60 min, 22°C	1) 5 min, 4°C 2) Distilled water, 3x22°C
	5-HT ₂	[³ H]-Ketanserin (1.14)	Mianserin (10 µM)	170 mM Tris-HCl (pH 7.7)	30 min, 22°C	120 min, 22°C	1) 2x10 min, 4°C 2) Distilled water, 3x22°C
Dopamine	D ₁	[³ H]-SCH 23390	SKF 83566 (1 µM)	50 mM Tris-HCl + 120 mM NaCl + 5 mM KCl + 2 mM CaCl ₂ + 1 mM MgCl ₂	20 min, 22°C	90 min, 22°C	1) 2x20 min, 4°C 2) Distilled water, 1x22°C
Adenosine	A ₁	[³ H]-DPCPX (1.0)	R-PIA (100 µM)	170 mM Tris-HCl + 2 Units/I Adenosine deaminase [+ 100 µM	15 min, 4°C	120 min, 22°C	1) 2x5 min, 4°C 2) Distilled water, 1x22°C

* Substances in square brackets only included in the main incubation

Supplementary Table 2. Statistic values (e.g., F value and p value) for the omnibus test (i.e., the first level test) of macaque and human early visual areas.

	Macaque		Human	
	F value	p value	F value	p value
Area	11.763	1.56E-14***	17.2632	2.20E-16***
Receptor	33.801	2.20E-16***	33.1286	2.20E-16***
Area \times Receptor	4.62	2.20E-16***	5.9207	2.20E-16***

* $p < 0.05$, ** $p < 0.01$, *** $p < 0.001$

Supplementary Table 3. Statistic values (e.g., F value and corrected p value) for the simple effect tests (i.e., the second level test) of macaque and human early visual areas.

	Macaque		Human	
	F value	p_{corr}	F value	p_{corr}
AMPA	3.262	0.0035**	2.24	0.0383*
kainate	8.452	0.0004***	4.267	0.0002***
NMDA	3.862	0.0009***	9.365	0.0002***
GABA _A	3.79	0.0009***	7.246	0.0002***
GABA _B	2.258	0.0323*	0.949	0.5032
GABA _A /BZ	3.735	0.0010**	4.126	0.0004***
M ₁	1.29	0.2517	5.289	0.0002***
M ₂	11.085	0.0004***	27.054	0.0002***
M ₃	2.739	0.0112*	2.126	0.0443*
α_1	2.543	0.0171**	2.22	0.0383*
α_2	17.587	0.0004***	13.795	0.0002***
5-HT _{1A}	6.896	0.0004***	12.354	0.0002***
5-HT ₂	2.928	0.0075**	3.217	0.0032**
D ₁	1.677	0.1193	0.802	0.5859

* $p < 0.05$, ** $p < 0.01$, *** $p < 0.001$

Supplementary Table 4. FDR-corrected p -values for the post hoc tests (i.e., third level tests) of macaque early visual areas. Correction was carried out for each receptor type separately (i.e., p -values were corrected for 28 comparisons per receptor type). Note, that no p -values are provided for the M₁ or D₁ receptors, because they did not reach the level of significance in the second level test.

Macaque	AMPA	kainate	NMDA	GABA _A	GABA _B	GABA _A /BZ	M ₂	M ₃	α_1	α_2	5-HT _{1A}	5-HT ₂
mV1d/mV1v	0.4234	0.7081	0.8546	0.8829	0.3327	0.0905	0.6412	0.4687	0.8008	0.6568	0.8803	0.7422
mV1d/mV2d	0.2893	0.0055**	0.0165*	0.1224	0.7651	0.0905	0.0001***	0.0134*	0.5152	0.0001***	0.0377*	0.035*
mV1d/mV2v	0.8509	0.2525	0.0461*	0.0986	0.2255	0.3029	0.0001***	0.0134*	0.5635	0.0001***	0.0274*	0.1005
mV1d/mV3A	0.0148*	0.8317	0.0108*	0.0118*	0.1207	0.0017**	0.0001***	0.0799	0.1564	0.0001***	0.0001***	0.0727
mV1d/mV3d	0.4234	0.5144	0.0165*	0.0135*	0.1207	0.0017**	0.0001***	0.0343*	0.9845	0.0001***	0.1852	0.0727
mV1d/mV3v	0.1301	0.0003***	0.011*	0.0118*	0.0276*	0.0102*	0.0001***	0.0343*	0.6063	0.0001***	0.0002***	0.4187
mV1d/mV4v	0.5632	0.0001***	0.0272*	0.0066**	0.2255	0.1062	0.0001***	0.2689	0.0868	0.0001***	0.0032**	0.438
mV1v/mV2d	0.8211	0.0186*	0.011*	0.2046	0.5907	0.6953	0.0001***	0.1255	0.6299	0.0001***	0.0274*	0.028*
mV1v/mV2v	0.4397	0.4315	0.0272*	0.1677	0.7651	0.7289	0.0001***	0.1362	0.4451	0.0001***	0.0228*	0.035*
mV1v/mV3A	0.1301	0.8317	0.0108*	0.0184*	0.6056	0.1062	0.0001***	0.4445	0.2308	0.0001***	0.0001***	0.0327*
mV1v/mV3d	0.9799	0.3314	0.011*	0.0225*	0.5907	0.0916	0.0001***	0.29	0.8008	0.0001***	0.14	0.0327*
mV1v/mV3v	0.4397	0.0012**	0.0108*	0.0185*	0.2542	0.368	0.0001***	0.2851	0.7864	0.0001***	0.0001***	0.2235
mV1v/mV4v	0.145	0.0001***	0.0165*	0.0105*	0.7651	0.8261	0.0001***	0.7432	0.1564	0.0001***	0.0022**	0.2451
mV2d/mV2v	0.4077	0.1549	0.8546	0.9481	0.3801	0.4878	0.9599	0.9528	0.2005	0.8017	0.8861	0.7422
mV2d/mV3A	0.1743	0.01*	0.8546	0.445	0.2542	0.3414	0.539	0.5624	0.5152	0.9482	0.0231*	0.8629
mV2d/mV3d	0.8211	0.0006***	0.9984	0.47	0.2377	0.3029	0.9599	0.7432	0.5152	0.9482	0.4531	0.875
mV2d/mV3v	0.5864	0.4315	0.8546	0.4535	0.0958	0.7289	0.8312	0.7522	0.8227	0.9482	0.1152	0.3605
mV2d/mV4v	0.1301	0.1437	0.8546	0.2052	0.3897	0.5568	0.6897	0.3031	0.3156	0.8746	0.4111	0.2857
mV2v/mV3A	0.0215*	0.3314	0.7098	0.47	0.7838	0.0916	0.4968	0.6085	0.0441*	0.6568	0.0274*	0.927
mV2v/mV3d	0.4397	0.061	0.8546	0.5236	0.7651	0.0905	0.9883	0.7522	0.5635	0.6568	0.4111	0.9161
mV2v/mV3v	0.145	0.0188*	0.8381	0.47	0.4112	0.3029	0.8198	0.7522	0.2572	0.6568	0.14	0.5247
mV2v/mV4v	0.4397	0.0018**	0.8546	0.2488	0.952	0.8261	0.6777	0.3322	0.0197*	0.5092	0.4531	0.4397
mV3A/mV3d	0.1301	0.4315	0.8546	0.9481	0.952	0.9193	0.4968	0.7703	0.1564	0.9736	0.0023**	0.9563
mV3A/mV3v	0.4377	0.0006***	0.8546	0.9596	0.5907	0.4878	0.6897	0.7522	0.4047	0.9736	0.4534	0.4397
mV3A/mV4v	0.0018**	0.0001***	0.8381	0.76	0.7651	0.0905	0.8312	0.7432	0.7864	0.9482	0.1496	0.4187
mV3d/mV3v	0.4397	0.0001***	0.8546	0.9481	0.6056	0.4406	0.8198	0.9528	0.6063	0.9736	0.0228*	0.438
mV3d/mV4v	0.145	0.0001***	0.8546	0.6892	0.7651	0.0905	0.6777	0.5624	0.0868	0.9482	0.1152	0.4187
mV3v/mV4v	0.0263*	0.4852	0.8546	0.7495	0.3982	0.3029	0.8408	0.5541	0.2308	0.9482	0.4531	0.9302

Pink background highlights pairs of adjacent early visual areas in the macaque brain. * $p < 0.05$, ** $p < 0.01$, *** $p < 0.001$

Supplementary Table 5. FDR-corrected p -values for the post hoc tests (i.e., third level tests) of human early visual areas. (i.e., p -values were corrected for 28 comparisons per receptor type). Note, that no p -values are provided for the GABA_B or D₁ receptors, because they did not reach the level of significance in the second level test.

Human	AMPA	kainate	NMDA	GABA _A	GABA _A /BZ	M ₁	M ₂	M ₃	α ₁	α ₂	5-HT _{1A}	5-HT ₂
hV1d/hV1v	0.4636	0.4866	0.8219	0.5618	0.2268	0.7741	0.908	0.4081	0.6365	0.9919	0.2632	0.3822
hV1d/hV2d	0.5712	0.0763	0.0299*	0.0027**	0.2317	0.089	0.0001***	0.9411	0.7442	0.0001***	0.0004***	0.7705
hV1d/hV2v	0.5712	0.8912	0.1249	0.0001***	0.0874	0.2536	0.0001***	0.4479	0.8992	0.0001***	0.0069**	0.0111*
hV1d/hV3A	0.9675	0.0003	0.0001***	0.0001***	0.0115*	0.0002***	0.0001***	0.9411	0.1968	0.0001***	0.0001***	0.0111*
hV1d/hV3d	0.5712	0.8694	0.001**	0.0001***	0.3401	0.0037**	0.0001***	0.4081	0.7643	0.0001***	0.0001***	0.1538
hV1d/hV3v	0.5712	0.3856	0.0538	0.0027**	0.8512	0.1501	0.0001***	0.4081	0.6365	0.0001***	0.0001***	0.3514
hV1d/hV4v	0.1537	0.1756	0.0001***	0.0001***	0.0681	0.0014**	0.0001***	0.4479	0.2427	0.0001***	0.0842	0.1538
hV1v/hV2d	0.1175	0.3134	0.0538	0.0159*	0.9593	0.1793	0.0001***	0.3006	0.8206	0.0001***	0.0001***	0.5244
hV1v/hV2v	0.1091	0.5833	0.201	0.0001***	0.6296	0.4278	0.0001***	0.0388*	0.547	0.0001***	0.0001***	0.1289
hV1v/hV3A	0.4636	0.0045**	0.0001***	0.0002***	0.2268	0.0009***	0.0001***	0.373	0.4167	0.0001***	0.0001***	0.1003
hV1v/hV3d	0.1091	0.6148	0.0019**	0.0008***	0.0222*	0.0119*	0.0001***	0.0388*	0.8014	0.0001***	0.0001***	0.5244
hV1v/hV3v	0.1091	0.8398	0.0832	0.0156*	0.3401	0.2575	0.0001***	0.0388*	0.2952	0.0001***	0.0001***	0.8535
hV1v/hV4v	0.5795	0.4866	0.0001***	0.0002***	0.3872	0.0046**	0.0001***	0.0618	0.1082	0.0001***	0.0094**	0.5098
hV2d/hV2v	0.9675	0.0957	0.5396	0.2066	0.6296	0.5948	0.1302	0.5898	0.6784	0.71	0.442	0.0219*
hV2d/hV3A	0.5795	0.1054	0.0023**	0.2123	0.2268	0.0295*	0.0017**	0.9411	0.2952	0.3	0.218	0.0176*
hV2d/hV3d	0.9675	0.0957	0.2649	0.4715	0.0274*	0.229	0.0112	0.4839	0.9498	0.7593	0.0766	0.2595
hV2d/hV3v	0.9675	0.4866	0.8553	0.9285	0.3649	0.7859	0.1262	0.4839	0.4167	0.6477	0.3511	0.5098
hV2d/hV4v	0.054	0.8398	0.0012**	0.1575	0.3872	0.0935	0.014*	0.5898	0.1388	0.0029**	0.3065	0.2595
hV2v/hV3A	0.5712	0.0003***	0.0003***	0.9908	0.4126	0.007**	0.1748	0.4839	0.149	0.5293	0.0456*	0.8535
hV2v/hV3d	0.9675	0.9446	0.0765	0.6471	0.0083**	0.0855	0.435	0.9411	0.6784	0.5144	0.0094**	0.3582
hV2v/hV3v	0.9675	0.4671	0.6459	0.2627	0.2011	0.7741	0.9673	0.9411	0.6784	0.9417	0.0842	0.1538
hV2v/hV4v	0.054	0.2174	0.0002***	0.7283	0.6296	0.0295*	0.4052	0.9411	0.2869	0.0095**	0.6678	0.5244
hV3A/hV3d	0.5712	0.0003***	0.0569	0.6471	0.0004***	0.3459	0.5759	0.4479	0.2952	0.1483	0.6678	0.3014
hV3A/hV3v	0.5712	0.0187*	0.002**	0.2651	0.0329*	0.0181*	0.1797	0.4479	0.108	0.5893	0.7172	0.1498
hV3A/hV4v	0.1537	0.0957	0.6184	0.7283	0.8575	0.7741	0.7695	0.4839	0.0126*	0.0648	0.0437*	0.5098
hV3d/hV3v	0.9675	0.4866	0.2176	0.5438	0.2806	0.1551	0.4425	0.9411	0.4167	0.4561	0.442	0.6207
hV3d/hV4v	0.054	0.2342	0.0267*	0.4801	0.0083**	0.5937	0.8931	0.9488	0.1388	0.0008***	0.0121*	0.8535
hV3v/hV4v	0.054	0.6725	0.0011**	0.205	0.1298	0.0686	0.4092	0.9411	0.4951	0.0121*	0.0766	0.5436

Pink background highlights pairs of adjacent early visual areas in the human brain. * $p < 0.05$, ** $p < 0.01$, *** $p < 0.001$

Supplementary Table 6. Absolute receptor densities (mean±sd in fmol/mg protein) of macaque and human early visual areas. Cells have been color-coded to facilitate identification of areas with higher (warm tones) and lower (cool tones) receptor densities.

	AMPA	kainate	NMDA	GABA _A	GABA _B	GABA _A /BZ	M ₁	M ₂	M ₃	α ₁	α ₂	5-HT _{1A}	5-HT ₂	D ₁
Macaque														
mV1d	285±34	483±38	1379±73	1889±268	1855±242	2344±305	865±352	342±82	840±109	249±55	466±24	63±25	404±80	78±11
mV1v	319±25	502±50	1392±54	1847±243	1723±252	2038±187	865±348	377±96	792±121	257±48	493±21	60±26	421±96	80±15
mV2d	327±67	613±29	1214±110	1615±362	1805±130	1889±13	940±227	175±45	704±86	271±51	300±12	102±21	321±83	70±4
mV2v	291±28	542±34	1242±53	1597±259	1682±206	2062±165	1078±22	179±54	708±67	231±53	319±44	104±31	338±77	68±5
mV3A	378±30	492±50	1187±30	1455±269	1653±275	1647±3	879±111	133±23	742±97	294±59	292±46	145±44	333±70	74±10
mV3d	318±46	452±38	1214±81	1477±378	1645±256	1628±19	907±87	179±60	728±69	250±41	295±26	88±34	331±72	75±5
mV3v	346±75	652±53	1197±119	1462±343	1575±174	1823±255	954±281	161±55	725±93	266±60	294±48	132±43	359±84	62±9
mV4v	264±60	686±80	1229±104	1389±388	1688±214	2073±363	823±332	148±46	765±104	303±46	285±63	118±34	369±73	73±21
Human														
hV1d	279±66	319±58	1484±317	2356±642	1757±177	1746±260	516±129	359±75	1004±424	339±86	853±180	149±47	344±48	104±23
hV1v	245±39	360±115	1474±305	2347±773	1686±176	1913±380	503±134	361±66	1204±359	351±102	830±208	127±23	331±28	106±23
hV2d	304±73	400±108	1314±250	1842±520	1595±250	2102±590	470±158	236±38	1017±187	349±100	583±106	206±45	338±62	97±24
hV2v	312±90	325±64	1352±289	1593±433	1640±340	2168±821	462±93	194±64	899±321	327±96	563±177	203±57	306±45	99±14
hV3A	281±79	509±246	1051±444	1624±662	1813±531	2368±921	327±63	162±57	1041±317	406±147	501±262	223±64	305±60	103±28
hV3d	315±109	332±59	1187±312	1704±653	1537±229	1548±256	401±108	184±46	827±271	351±91	613±107	238±70	315±50	97±22
hV3v	327±110	377±82	1266±395	1875±602	1773±339	1783±283	451±112	214±97	859±263	304±82	557±100	228±60	324±49	98±27
hV4v	181±60	390±119	945±404	1467±565	1772±633	2181±904	332±85	155±42	904±143	274±116	299±144	184±51	298±69	87±22

Supplementary Table 7. Z-score normalized receptor densities used for cluster analyses depicted in [Figure 8](#). Note, that for each receptor type normalization was carried out separately for macaque and human areas. The datasets were transposed to carry out the cluster analyses shown in [Supplementary Fig. 8](#). Cells have been color-coded to facilitate identification of areas with higher (warm tones) and lower (cool tones) densities than the average for the respective receptor type.

	AMPA	kainate	NMDA	GABAA	GABA _B	GABAA/BZ	M ₁	M ₂	M ₃	α_1	α_2	5-HT _{1A}	5-HT ₂	D ₁
Macaque														
mV1d	-0.03	-0.94	1.18	1.50	0.62	-0.84	1.15	1.52	0.28	0.03	1.42	-1.16	1.43	0.87
mV1v	-0.73	-0.26	1.12	1.48	-0.10	-0.23	0.97	1.55	1.91	0.34	1.30	-1.73	0.65	1.20
mV2d	0.49	0.38	0.29	-0.03	-1.03	0.46	0.52	0.03	0.39	0.29	-0.09	0.29	1.05	-0.39
mV2v	0.65	-0.83	0.49	-0.77	-0.58	0.70	0.40	-0.47	-0.58	-0.26	-0.21	0.20	-0.85	0.01
mV3A	0.02	2.15	-1.09	-0.68	1.18	1.43	-1.46	-0.86	0.59	1.76	-0.56	0.71	-0.92	0.75
mV3d	0.71	-0.73	-0.38	-0.44	-1.62	-1.56	-0.44	-0.60	-1.16	0.36	0.07	1.12	-0.31	-0.37
mV3v	0.97	0.01	0.03	0.07	0.77	-0.70	0.25	-0.24	-0.90	-0.87	-0.24	0.84	0.24	-0.08
mV4v	-2.08	0.21	-1.64	-1.14	0.77	0.75	-1.39	-0.94	-0.54	-1.65	-1.69	-0.28	-1.30	-1.99
Human														
hV1d	-0.03	-0.94	1.18	1.50	0.62	-0.84	1.15	1.52	0.28	0.03	1.42	-1.16	1.43	0.87
hV1v	-0.73	-0.26	1.12	1.48	-0.10	-0.23	0.97	1.55	1.91	0.34	1.30	-1.73	0.65	1.20
hV2d	0.49	0.38	0.29	-0.03	-1.03	0.46	0.52	0.03	0.39	0.29	-0.09	0.29	1.05	-0.39
hV2v	0.65	-0.83	0.49	-0.77	-0.58	0.70	0.40	-0.47	-0.58	-0.26	-0.21	0.20	-0.85	0.01
hV3A	0.02	2.15	-1.09	-0.68	1.18	1.43	-1.46	-0.86	0.59	1.76	-0.56	0.71	-0.92	0.75
hV3d	0.71	-0.73	-0.38	-0.44	-1.62	-1.56	-0.44	-0.60	-1.16	0.36	0.07	1.12	-0.31	-0.37
hV3v	0.97	0.01	0.03	0.07	0.77	-0.70	0.25	-0.24	-0.90	-0.87	-0.24	0.84	0.24	-0.08
hV4v	-2.08	0.21	-1.64	-1.14	0.77	0.75	-1.39	-0.94	-0.54	-1.65	-1.69	-0.28	-1.30	-1.99

Supplementary Table 8. Z-score normalized receptor densities used for cluster analyses depicted in [Figure 9](#). Note, that for each receptor type normalization was carried out together for macaque and human areas. Cells have been color-coded to facilitate identification of areas with higher (warm tones) and lower (cool tones) densities than the average for the respective receptor type.

	AMPA	kainate	NMDA	GABAA	GABA _B	GABAA/BZ	M ₁	M ₂	M ₃	α_1	α_2	5-HT _{1A}	5-HT ₂	D ₁
mV1d	-0.30	0.16	0.85	0.57	1.70	1.55	0.74	1.39	-0.14	-1.07	-0.03	-1.44	1.88	-0.52
mV1v	0.45	0.32	0.95	0.43	0.25	0.33	0.74	1.81	-0.47	-0.92	0.11	-1.49	2.37	-0.40
mV2d	0.65	1.27	-0.31	-0.36	1.15	-0.27	1.03	-0.55	-1.08	-0.62	-0.91	-0.79	-0.54	-1.08
mV2v	-0.16	0.67	-0.11	-0.42	-0.19	0.42	1.56	-0.50	-1.05	-1.45	-0.81	-0.75	-0.05	-1.20
mV3A	1.78	0.24	-0.50	-0.90	-0.52	-1.24	0.79	-1.04	-0.82	-0.16	-0.95	-0.05	-0.21	-0.79
mV3d	0.44	-0.11	-0.31	-0.83	-0.60	-1.32	0.90	-0.51	-0.92	-1.06	-0.94	-1.02	-0.26	-0.73
mV3v	1.07	1.61	-0.43	-0.88	-1.37	-0.54	1.08	-0.72	-0.93	-0.73	-0.94	-0.28	0.55	-1.60
mV4v	-0.77	1.90	-0.21	-1.13	-0.14	0.46	0.58	-0.87	-0.66	0.04	-0.99	-0.51	0.87	-0.85
hV1d	-0.42	-1.25	1.60	2.15	0.63	-0.85	-0.61	1.59	1.00	0.77	2.02	0.02	0.13	1.24
hV1v	-1.17	-0.90	1.52	2.12	-0.15	-0.18	-0.66	1.62	2.38	1.02	1.90	-0.35	-0.26	1.37
hV2d	0.13	-0.56	0.39	0.41	-1.15	0.58	-0.78	0.15	1.09	0.98	0.59	0.99	-0.06	0.74
hV2v	0.30	-1.20	0.66	-0.44	-0.66	0.85	-0.82	-0.33	0.27	0.54	0.49	0.93	-1.00	0.90
hV3A	-0.38	0.38	-1.46	-0.33	1.24	1.64	-1.34	-0.70	1.26	2.15	0.16	1.27	-1.03	1.19
hV3d	0.37	-1.14	-0.50	-0.06	-1.78	-1.64	-1.05	-0.45	-0.23	1.03	0.75	1.54	-0.73	0.75
hV3v	0.64	-0.75	0.06	0.52	0.80	-0.70	-0.86	-0.10	0.00	0.05	0.45	1.35	-0.46	0.87
hV4v	-2.61	-0.64	-2.21	-0.86	0.79	0.90	-1.32	-0.78	0.30	-0.57	-0.91	0.60	-1.22	0.11